PERGAMON

Progress in Surface Science 71 (2003) 95–146

Progress in SURFACE SCIENCE

www.elsevier.com/locate/progsurf

Properties of large organic molecules on metal surfaces

Federico Rosei [a,*], Michael Schunack [a], Yoshitaka Naitoh [a], Ping Jiang [b], André Gourdon [b], Erik Laegsgaard [a], Ivan Stensgaard [a], Christian Joachim [b], Flemming Besenbacher [a]

[a] *Interdisciplinary Nanoscience Center (i NANO) and Department of Physics and Astronomy, University of Aarhus, Ny Munkegade building 520, 8000 Aarhus C, Denmark*

[b] *CEMES–CNRS, 29 Rue J. Marvig, 31055-F Toulouse Cedex, France*

Abstract

The adsorption of large organic molecules on surfaces has recently been the subject of intensive investigation, both because of the molecules' intrinsic physical and chemical properties, and for prospective applications in the emerging field of nanotechnology. Certain complex molecules are considered good candidates as basic building blocks for molecular electronics and nanomechanical devices. In general, molecular ordering on a surface is controlled by a delicate balance between intermolecular forces and molecule–substrate interactions. Under certain conditions, these interactions can be controlled to some extent, and sometimes even tuned by the appropriate choice of substrate material and symmetry. Several studies have indicated that, upon molecular adsorption, surfaces do not always behave as static templates, but may rearrange dramatically to accommodate different molecular species. In this context, it has been demonstrated that the scanning tunnelling microscope (STM) is a very powerful tool for exploring the atomic-scale realm of surfaces, and for investigating adsorbate–surface interactions. By means of high-resolution, fast-scanning STM unprecedented new insight was recently achieved into a number of fundamental processes related to the interaction of largish molecules with surfaces such as molecular diffusion, bonding of adsorbates on surfaces, and molecular self-assembly. In addition to the normal imaging mode, the STM tip can also be employed to manipulate single atoms and molecules in a bottom–up fashion, collectively or one at a time. In this way, molecule-induced surface restructuring processes can be revealed directly and nanostructures can be engineered with atomic precision

* Corresponding author. Present address: INRS Énergie, Matériaux et Télécommunications, Université du Québec, 1650 Boul. Lionel Boulet, Varennes (QC), Canada J3X 1S2. Tel.: +1-450-9298246; fax: +1-450-9298102.

E-mail address: rosei@inrs-emt.uquebec.ca (F. Rosei).

0079-6816/03/$ - see front matter
doi:10.1016/S0079-6816(03)00004-2

to study surface quantum phenomena of fundamental interest. Here we will present a short review of some recent results, several of which were obtained by our group, in which several features of the complex interaction between large organic molecules and metal surfaces were revealed. The focus is on experiments performed using STM and other complementary surface-sensitive techniques.

Keywords: Molecular electronics; Surface diffusion; Molecular mechanics; Molecular conformations; Surface reconstruction; Self-assembly; Scanning tunneling microscopy; Scanning probe microscopy; Elastic scattering quantum chemistry

Contents

1. Introduction

New ways have to be explored if the miniaturization of electronic devices is to continue at the same pace as in the last decades. Besides incurring in exponentially increasing fabrication costs, the down-scaling of (optical) lithographic processes in the "top–down" approach for silicon chip manufacturing will soon lead to fundamental physical limits [1]. An alternative possibility is to explore the so-called "bottom–up" approach, which is based on the formation of functional devices out of prefabricated molecular building blocks with intrinsic electronic properties—an area generally referred to as molecular electronics [2]. Molecules can be considered as the ultimate limit of electronic devices, since their size is about 1 nm [3]. By using appropriately designed largish molecules, the density of transistors per chip might potentially be increased by up to a factor of 10^5 compared to present standards.

The possibility of tailoring organic molecules with particular properties, the tunability of their characteristics, and the efficiency and flexibility of deposition methods, are considered valid reasons for a strong effort to show their applicability as competitive materials with respect to e.g. inorganic semiconductors. This is explored in areas such as molecular electronics [2], nanodevices [4], and molecular recognition [5] and as a result, molecular materials have been employed to develop solar cells [6], gas sensors [7], heterojunctions [8], and ultrafast optical switches [9].

At the same time, in the field of optoelectronics, aromatic molecules are important, since they have the property of absorbing electromagnetic radiation in the visible range. In addition to giving them intense, bright colors [10], this feature also makes them interesting candidates as dyes in light-emitting devices. This was shown for example in the case of decacyclene (DC) as dopant in an electroluminescent device with high luminance and a long lifetime [11] and a light-emitting diode (LED) based on Langmuir–Blodgett films [12]. Other practical applications of optoelectronic devices as photodiodes require the use of inexpensive organic thin films [13,14]. A thorough understanding of growth and crystallization of molecules on surfaces is essential to tailor emission processes in a desired way, which in turn is crucial for device optimization.

In all cases molecule–surface interaction plays a vital role, since the binding and ordering of molecules on surfaces is in general controlled by a delicate balance

Nomenclature

AES	Auger electron spectroscopy
AFM	atomic force microscopy/microscope
C_{60}	Buckminster fullerene
CuPc	Cu-phthalocyanine
DC	decacyclene
ESQC	elastic scattering quantum chemistry
FIM	field ion microscopy
HtBDC	hexa-di-*tert*-butyl decacyclene
LEED	low energy electron diffraction
OMBD	organic molecular beam deposition
PVBA	4-*trans*-2-(pyrid-4-yl-vinyl) benzoic acid
SAM	self-assembled monolayer
SPM	scanning probe microscopy
STM	scanning tunneling microscopy/microscope
STS	scanning tunneling spectroscopy
TBPP	*tert*-butylphenyl
TDS	thermal desorption spectroscopy
UHV	ultra high vacuum
XPD	X-ray photoelectron diffraction
XPS	X-ray photoelectron spectroscopy

between competing molecule–substrate and intermolecular interactions. Non-covalent molecule–molecule interactions are often believed to dominate over molecule–surface interactions, and metal substrates are often considered as static checkerboards that simply provide bonds and specific adsorption sites to the molecules [15–18]. However, when adsorbing large organic molecules on metal substrates, the complexity of the molecule–surface interaction often increases dramatically. For example, several studies have indicated that there may be a restructuring of the substrate underneath the molecular adsorbate layer [19,20].

As another consequence of the complex interactions involved, certain molecular behavior, although valid for molecules in the gas phase, cannot be transferred a priori to a situation in which molecules are adsorbed on a substrate. For example, the exact adsorption conformation may play an important role when measuring the conductance through a single molecule [21–24]. Similarly, molecular electromechanical devices use the effects of mechanical deformation on the electrical properties of molecules. It is therefore important to understand in detail the binding geometry of the molecules on the surface at hand, and the interactions that may induce molecular anchoring to the substrate and play a central role in molecular motion along the surface. So far there are only few studies of molecular conformations for complex molecules [4,25–28].

In the last two decades the STM has become a very versatile and important tool in the area of surface and nanoscale science. While the STM was originally developed for gaining invaluable information on the atomic-scale structure of pristine metal and semiconductor surfaces [29–33], it has subsequently been used, for example, for detailed studies of the properties of adsorbates on metals [31,32], for monitoring growth processes in situ [31,33], and for observing the conformations of large organic molecules on various substrates [34]. Most recently, advances in instrumentation have turned the STM into a unique tool for manipulating nanoscale objects such as single atoms and molecules on a surface, including lateral displacements and vertical transfer. Furthermore, it has been demonstrated that single chemical bonds can be broken and formed selectively by means of an STM tip [35–38]. The ability to manipulate matter with atomic-scale precision provides not only a new avenue for forming artificial, ordered structures at the nanoscale [39], but can also be used to gain fundamental new insight into the detailed binding and ordering of molecules on surfaces, leading to precious new information on the nature of chemical bonds [40]. Other valuable insight into molecule–surface interactions can be gained from a variety of other surface sensitive techniques such as Auger electron spectroscopy (AES), low energy electron diffraction (LEED), and X-ray photoelectron spectroscopy (XPS). However, in general the information obtained from these techniques is averaged over large areas of the sample substrate compared to the characteristic molecular distances on the surface. This clearly limits the ability to yield information on local properties, which is essential in the present context.

In this review we will mainly address how high-resolution STM can contribute to investigate fundamental questions in relation to the adsorption of fairly large (a few hundred atoms at most) organic molecules at metal surfaces [34]. Most of the molecules described in the following pages can be considered prototypes in the area of molecular electronics, designed to act as nanoscale devices (e.g. as molecular wires) [41]. All the experiments reported hereafter were carried out under ultra high vacuum (UHV) ambient conditions and molecules were transferred onto metal substrates by organic molecular beam deposition (OMBD). The results that will be presented in this article are grouped in topics covering different aspects of molecule–surface interaction.

We start out by describing in Section 2 elastic scattering quantum chemistry (ESQC) calculations, which, when combined with STM imaging, have led to detailed results on investigations of molecule–surface interactions. Section 3 addresses how the conformations of single molecules are changed when the molecules adsorb on surfaces and in Section 4 we briefly review some manipulation experiments which led to new insight into conformational details of molecules adsorbed on surfaces. Molecular surface diffusion [42–44] as a prerequisite for molecules to meet on a surface and to eventually form ordered structures is discussed in Section 5. In this context, fast-scanning STMs have permitted significant advances. That the bonding and ordering of molecules on surfaces can indeed also be governed by molecule–substrate interactions [45,46] is the content of Section 6. Finally, the formation of self-assembled monolayers (SAMs) on metal surfaces, i.e. the bonding and ordering of

molecules on surfaces will be discussed in Section 7 in a few selected cases [15,20,47–49].

The literature in the field of large organic molecules, especially in the area of SAMs is too extensive to be treated thoroughly in the context of the present review and we will therefore use many results obtained in the framework of the collaborations initiated through the European IST Project "BUN" and the TMR Network "AMMIST".

Other groups [50–54] have conducted similar studies by adsorbing organic molecules on semiconductor surfaces, but this is also outside the scope of this review, limited as it is to metal surfaces only.

2. Elastic scattering quantum chemistry calculations

The study of largish organic molecules on surfaces by scanning probe microscopy (SPM) has required the development of sophisticated theoretical tools for the interpretation of SPM images. Atomic adsorbates usually induce a perturbation of the local density of states (LDOS) on a surface, thereby causing new features (depressions or protrusions) to appear in STM images [31]. The perturbation induced by large organic molecules is often much stronger, due to their more complex physical and chemical properties. In this case we make direct use of the fact that the STM measures the molecule's local *transparency* to tunneling electrons, giving a *characteristic local tunneling footprint*, from which important information may be deduced. STM images of conjugated molecules are often dominated by quantum interference effects, which may hinder the overall resolution of the actual molecular shape [55].

The most advanced theoretical technique in this context is undoubtedly the elastic scattering quantum chemistry or ESQC routine, which allows a calculation from first principles of simulated SPM images [56–58]. This technique is often used together with a standard molecular mechanics (MM2) routine, to optimize the structural rigidity and conformations of the molecules on the substrate at hand. The calculations include electronic coupling with the substrate.

The ESQC routine is based on the calculation of the full scattering matrix of the STM tunnel junction as scans over the whole molecule. The description of this junction encompasses the surface, the adsorbate, the tip apex, and both the bulk material supporting the tip apex and the surface. Whatever the tip apex position, several hundred molecular orbitals are used to describe the electronic properties of the junction with the organic molecule positioned under the tip apex. The surface atoms and the organic molecule are described taking into account all valence molecular orbitals.

Electronic interactions inside the junction are calculated using a semi-empirical extended Hückel approximation with a double zeta basis set, in order to properly reproduce the tip apex wave function in space away from the tip apex end atom. The MM2 routine used in conjunction with ESQC to optimize molecular geometries in the tunnel junction is a standard MM2 routine with a generalized potential for surface metal atoms.

3. Conformations of large organic molecules on a metal surface

The structure of a molecule and its several possible conformations when adsorbed on a substrate ultimately determine its chemical and physical properties. When large molecules are adsorbed on a metallic substrate, where they extend over a considerable number of sites, they must adapt to surface chemistry, geometry and corrugation, and it can be expected a priori that their internal configurations will vary—sometimes substantially—as a result of the interaction.

Molecular conformation at interfaces is very important in organic thin films, and particularly in organic optoelectronic devices, since it may affect the ultimate properties and performance of a device. As a result of the adsorption process, strong molecule–surface interaction may induce conformational changes within the molecule, sometimes causing severe distortions, which in turn may affect its overall characteristics. In fact, conformational changes can be induced not only by the chemical properties of the substrate, but also by its geometrical structure. It is therefore necessary to have detailed information on the binding geometry of the molecules on the substrate of choice. So far, molecular conformations have been the subject of only a few selected studies [4,25–28]. In the following, we will describe in some detail some recent experimental and theoretical results that have led to significant insight into conformational changes of large organic molecules on metallic surfaces. The focus is on porphyrin-based molecules and molecules from what is termed the ''Lander'' family (model systems that are designed to act as ''molecular wires'', so named because of their resemblance to a molecular-scale interplanetary spacecraft, similar to the Mars Lander), all of which have a conducting backbone made of a π-system. We will show that in general the leading molecule–substrate interaction is determined by the attraction between the π-system and the underlying surface, which often causes distorted configurations in the observed molecular shapes. This information is important because it points to the necessity and possibility of custom-designing molecules to confer upon them predefined properties upon adsorption.

3.1. Porphyrin-based molecules

Among the great number of compounds that have been proposed as useful molecular materials, porphyrins have an important role, for example because of their efficiency in solar energy conversion. Porphyrins are also model systems to study charge transfer and in vivo photoactivation of drug precursors, and have been employed in organic light-emitting devices. At the same time, they are candidates for molecular electronics or mechanical devices, as exemplified by their recent use as a molecular switch [4]. The properties of porphyrins can be fine-tuned by modifying their molecular skeleton, and a large number of porphyrin analogues have been synthesized for this purpose (e.g. sapphyrin). Indeed, the demonstration of a close relationship between structure and properties opens new perspectives in the synthesis of macrocycles with a controlled behavior, which renders these molecules particularly interesting for applications [59,60].

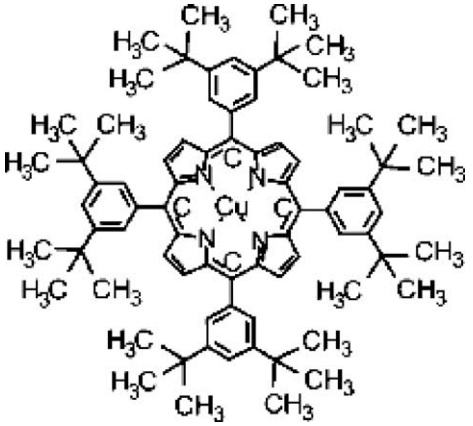

Fig. 1. Chemical structure of Cu-TBPP.

Cu-tetra[3,5-di-*tert*-butylphenyl] porphyrin (abbreviated as Cu-TBPP in the following) is a specially designed porphyrin-based molecule [4] with four phenyl-based lateral groups (Fig. 1). It belongs to a class of porphyrins in which the phenyl-based substituents are symmetrically bound, interconnecting carbon atoms on pyrrole rings (Fig. 1). These spacer groups effectively act as ''legs'', which physically separate the porphyrin central ring from the substrate, leading to an electronic decoupling of the molecule's central ring. In the gas phase these legs are generally oriented perpendicular to the plane of the central ring, but they are free to rotate around the σ bond, which connects each of them to the porphyrin center. The overall conformation of TPP derivatives is generally ascribed to a steric repulsion between the *ortho*-substituents on the phenyl ring and the external substituents on the pyrrole ring. This repulsion partially determines the rotation of the phenyl groups, together with the competing effect of the degree of π overlap with the porphyrin ring. The rotation angle around each of the four phenyl–porphyrin bonds is the predominant conformational factor that ultimately determines the shape of Cu-TBPP when adsorbed on a surface, as will be described hereafter.

3.1.1. Adsorption of Cu-TBPP on various metal substrates (Au(1 1 0), Cu(0 0 1), Cu(1 1 1), Cu(2 1 1), Ag(1 1 0))

STM images of Cu-TBPP in its adsorbed state on a metal surface typically consist of four bright lobes, although eight lobes appear in some cases due to a stronger molecule–substrate interaction. By varying polarity and magnitude of the bias voltage, no significant changes in the appearance of Cu-TBPP in STM images are observed, indicating (among other things) that in this case the STM measures real, not apparent, distances, and heights. The distances between the lobes, their dimensions and the theoretical STM-ESQC calculations confirm that these features correspond to tunneling through the four di-*tert*-butylphenyl (DBP) substituents, which are in direct contact with the substrate. The central porphyrin part does not

contribute noticeably to the image because it is well elevated above the surface, and it is therefore thought to be electronically decoupled from the substrate. As we will see in the following, contrast in the STM images for molecules of the Lander family is also always dominated by tunneling through molecular spacer groups. The conducting part is generally transparent to tunneling electrons, since tunneling occurs perpendicular to the π-system (whereas conduction is expected to take place horizontally, along the aromatic part).

It has been shown that Cu-TBPP adapts conformationally to different metallic substrates, or to different local geometries on the same metal, by rotating the σ bonds of the four DBP groups, which are symmetrically attached to the central part of the molecule. These four bulky groups including their orientation are ultimately responsible for the image shape of the molecule in STM topographies, and can give rise to either four or eight bright lobes (two lobes per spacer group in this case) depending on substrate structure and chemistry.

When deposited on atomically clean Au, Ag or Cu substrates, these four lobes have been observed to form different patterns. These patterns are directly related to the rotation angles of the DBTP substituents, depending on surface chemistry and orientation (ranging from 90° on Cu(0 0 1) to 45° on Ag(1 1 0) to flat on Cu(1 1 1) and Cu(2 1 1)). As remarked above and as will be discussed below, these results show that surface chemistry *and* surface geometry play a significant role in determining molecular conformations on a substrate.

On atomically clean Au(1 1 0), three characteristic shapes of Cu-TBPP can be identified in STM images, corresponding to no less than three different geometrical arrangements of the four lobes. It is observed that the different conformations of the molecules are uniquely related to their aspect ratios (defined as the height to base ratio). The shape of the four quadrilateral lobes at each molecule, which is in turn uniquely defined by their aspect ratio, is found to vary significantly between the three characteristic shapes identified on this substrate. The relative position of each of the four uppermost *tert*-butyl groups is determined by the rotation angle of the phenyl–porphyrin bond of each DBP substituent. The prominent features observed in STM images are consistent with an antisymmetric rotation of two opposite DBP substituents.

Jung et al. [26] observed two different rotations when adsorbing Cu-TBPP on Au(1 1 0), corresponding to an antisymmetric tilt of two opposite side groups by 65° and 45°, respectively. The 65° rotation is predominant after short annealing times (<10 min), and therefore this conformation was assigned to a metastable precursor state. On the other hand, the 45° form is predominant after longer annealing cycles, and is thought to be the thermodynamically stable configuration for this system. Remarkably, the adsorption of Cu-TBPP on Ag(1 1 0) yields the most pronounced conformational change. In this case a single adsorption state was observed, with a leg rotation of 45°.

From their extensive analysis, Jung et al. [26] concluded that molecular conformations of Cu-TBPP on different metal surfaces are mainly driven by the nature of molecule–substrate interaction. Later studies confirmed and extended this analysis, showing that this interaction depends both on substrate chemistry and geometry [27].

In contrast to the behavior just described, when adsorbed on Cu(0 0 1) the Cu-TBPP molecule retains a conformation similar to that of minimum energy for Cu-TBPP in vacuum i.e., a perpendicular orientation, with all four DBP groups rotated by 90° with respect to the porphyrin plane (the "board"). The square pattern of the lobes on this surface has the same symmetry as the face-centered-cubic(1 0 0) substrate, but is slightly rotated with respect to the [0 1 0] direction. In this case, the almost perpendicular orientation of DBP substituents is completely consistent with ESQC calculations. Surface geometry therefore seems to be the predominant effect in determining the adsorption conformation of Cu-TBPP on this substrate, since it allows the spacer groups to keep a rigid binding to the central part of the molecule.

With change of Cu surface orientation, from (0 0 1) to (1 1 1) or (2 1 1), i.e., with the same chemistry but a very different geometrical structure, the situation is completely different. On these surfaces, Cu-TBPP exhibits three different orientations in STM images, which follow the close-packed directions of the substrate. What is seen is the threefold 120° spatial symmetry of the *substrate*: the fourfold symmetry of the molecule has been broken, to allow the molecule to adapt itself to substrate geometry. In addition, because the legs are completely rotated parallel to the porphyrin plane, and both of the two end butyl groups of each leg can thus interact strongly with the surface, one sees *two* STM lobes per leg (yielding eight lobes per molecule), in STM images. (We will return to this topic in Section 4.2 where an eight-spot image is shown in Fig. 5.) On the Cu(2 1 1) surface, the TBPP molecules lie nearly flat, adopting two different rotational orientations relative to the step direction.

3.2. Molecular wires: "Conducting rods with legs"

In the context of molecular electronics, a molecular wire can be thought of as a long, linear molecule, which should have a small HOMO–LUMO gap and a specific organization of molecular energy levels, in order to guide tunneling electrons over long distances [61]. Currently several series of molecular rods with length up to 15 nm are available by means of chemical synthesis, but unfortunately they have a large HOMO–LUMO gap and consequently, poor electron transport properties [62]. Efficient long-distance molecular wires still represent a challenge for organic chemistry [63,64].

Model prototypes of molecular wires are generally equipped with so-called lateral or "spacer" groups, for several reasons:

(1) to increase solubility during chemical synthesis;
(2) to protect the integrity of the wire's molecular orbits when deposited on a substrate;
(3) to insulate wires from each other, in order to avoid cross-talk during electrical measurements.

In the case of spatially resolved conductance measurements along a so-called "Lander" molecular wire [21], the spacer groups were used as separation legs to adapt the height of one extremity of the wire to the contacting metal step edge.

Lander molecules were designed to act as interconnects between different nanodevices operating on an appropriate substrate.

In the following two subsections (Sections 3.2.1 and 3.2.2) we will describe a few selected studies related to the adsorption of different molecules of the Lander family on Cu substrates.

3.2.1. Adsorption of Single Landers on Cu(1 1 0) and Cu(0 0 1)

Recently, the adsorption of a large "four-legged" molecule named "Single Lander" (SL, $C_{90}H_{98}$, see Fig. 2A and B) [21,41,48] was studied in detail on clean Cu(1 1 0) [41] and Cu(0 0 1) [65] surfaces.

The Lander molecule is a standard prototype of a molecular device, in this case a molecular wire. It is about 17 Å long and 15 Å wide and consists of a conducting board (π-system) 4.5 Å wide and four "spacer legs" that elevate the board from the substrate (Fig. 2A and B). The legs are designed in such a way as to elevate the central part of the molecule by a nominal distance of 5 Å above the substrate upon adsorption (assuming an unperturbed conformation as in the gas phase). This separation should then electrically isolate the board from the surface, so that the Lander board may ideally act as a molecular wire segment, even when adsorbed on a metallic support.

In the gas phase the molecule can adopt different minimum-energy conformations, because the spacer groups can to some extent rotate around the σ bond

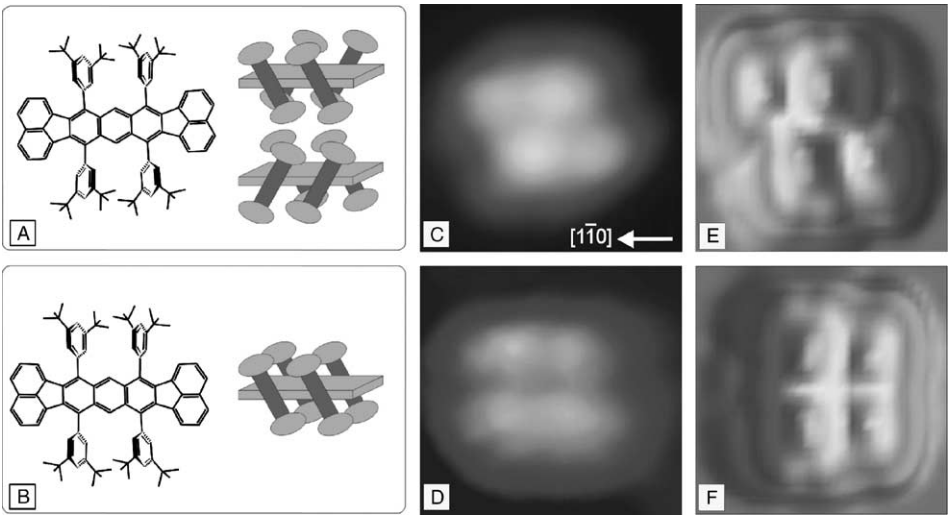

Fig. 2. Chemical structure and space-filling model of the Lander molecule in the (A) rhomboidal and (B) rectangular shape. STM image of a Lander molecule on Cu(1 1 0) at 100 K (2×2 nm^2, $V_t = -1000$ mV, $I_t = -0.21$ nA) with (C) rhomboidal shape and (D) rectangular shape. (E and F) ESQC-calculated STM images of the rhomboidal (chiral) and rectangular (achiral) Lander molecules, respectively, using the same tunneling parameters as in the experiments. The aromatic board of the Lander molecules is parallel to the close-packed Cu direction indicated in the image. From Ref. [41], with permission.

connecting them to the central board. The preferred conformation is attained by a rotation of the spacer legs out of the right-angled orientation to the board plane, which increases the π–π overlap between the aromatic core and the benzene units.

The STM images of SLs on both Cu(1 1 0) and Cu(0 0 1) appear as clusters of four bright lobes arranged in a quadrilateral geometry. We first consider the adsorption of SLs on Cu(1 1 0).

As shown in Fig. 2A and B, on Cu(1 1 0) the lobes are arranged in three possible conformations, one rectangular achiral shape and two rhomboidal chiral shapes. At room temperature (RT) on Cu(1 1 0) the molecules diffuse rapidly across the surface and are often imaged at step edges, from which one concludes that step edges are regions from which diffusion is difficult if not impossible. This adsorption is accompanied by the formation of Cu nanostructures protruding from the step edge, to which the molecules are effectively anchored [41]. This remarkable surface restructuring, which is not observed on Cu(0 0 1), will be discussed in detail in a later section (Section 6) of this review.

Upon adsorption on a Cu surface, the spacer legs of the SL molecule can react to the tendency of the board to be attracted to the surface in different ways. On each side of the axis, because of their mutual repulsion, the two legs must move in step, but more or less independently of the pair on the other side. Thus the two spacer groups on each side of the center board can each be tilted in one of two ways out of the right-angled orientation. Hence on the surface there are three minimum-energy conformations: two chiral (left- or right-handed) enantiomorphic (mirror-image) forms with C_{2h} symmetry (each with crossed or *staggered* conformation of legs on opposite sides of the board), Fig. 2A) and one achiral form with C_2 symmetry (self-mirroring) (*eclipsed* conformation of legs on opposite sides of the board, Fig. 2B).

In Fig. 2C and D we present a low temperature (LT, 100 K), high-resolution STM image of a Single Lander molecule deposited on Cu(1 1 0) and the corresponding calculated images in Fig. 2E and F [41]. Based on ESQC calculations [41,56], the two different molecular shapes (rectangular and near-rhomboidal) found in the STM images are in turn related to the two possible geometrical conformations of the molecule on the surface. In one conformation (see Fig. 2A), each pair of legs on the same side of the wire axis are parallel to each other but crossed with respect to the pair on the other side of the axis, giving an STM skewed parallelogram shape for four regions of tunneling "contact" of the spacer groups. This is a *chiral* form, since there are, of course, two ways ("left" and "right") to do the skewing. In the other *achiral* form, with the four legs all parallel to each other (Fig. 2B), only one rectangular shape for the four lobes is observed in the images. While there is only one image form (one only sees the "feet") there are two opposite ways to lean the "tops", so when two adsorbed molecules are adjacent along their axes, there will be a different interaction between them according to whether their "tilts" are parallel or antiparallel.

Turning now to the adsorption behavior of SL molecules on Cu(0 0 1), these were investigated by Kuntze et al. [65]. The aim of this experiment was to show that the SL acts as a molecular wire segment when contact is made to an atomic step. Comparison of experimental and ESQC-calculated STM images allowed the estab-

lishment of the detailed conformations of molecules adsorbed on terraces and at single atomic steps. It was inferred that the spacer legs are now not only rotated but are also significantly deformed due to the interaction of the molecule's central wire with the surface. This causes the central board to approach the surface until it rests only 0.37 nm above the topmost layer, compared to 0.7 nm for the unperturbed molecule. As a consequence of this reduction in stand-off distance, at monoatomic steps, this molecule is stabilized with the wire axis parallel to the edge, which unfortunately prevents good electronic contact between the wire's end groups and the upper terrace. Based on these observations, Kuntze et al. [65] conclude that constructing a molecule with more rigid legs could be a way to favor adsorption with the molecule oriented perpendicular to atomic steps, thereby allowing a better conduction across the steps.

3.2.2. Adsorption of Violet Lander molecules on Cu(0 0 1)

The Violet Lander (VL) (chemical structure reported in Fig. 3) is another prototype of molecular wire, from the same family as the Single Lander, but with a longer central "board". In a recent letter, Zambelli et al. [28] reported STM

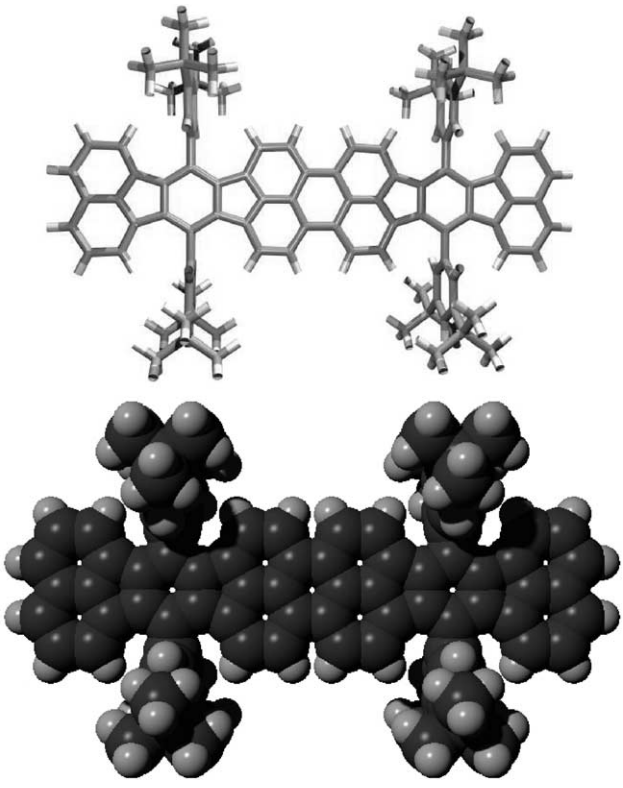

Fig. 3. Chemical structure of the Violet Lander. Top: stick model; bottom: space-filled model.

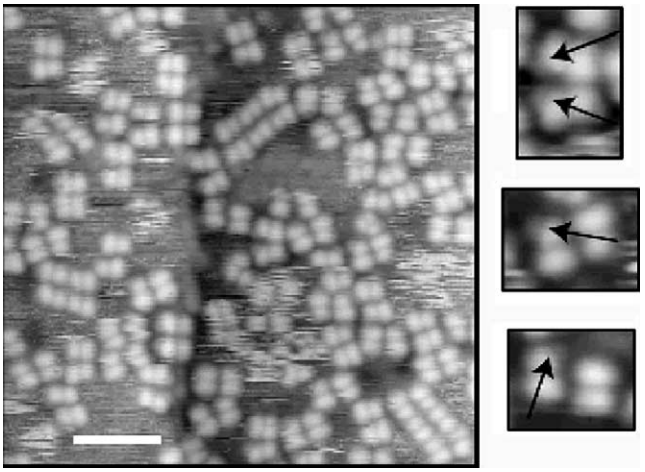

Fig. 4. STM image ($I_t = 10$ pA, $V_t = 2.5$ V) of VLs adsorbed on Cu(0 0 1). The white scale bar on the bottom left corresponds to 5 nm. The arrows on the zoomed molecules in the insets point to "shoulder" features. From Ref. [28], with permission.

observations of VLs on Cu(0 0 1), supported by ESQC calculations for extracting molecular conformations.

An STM image of a large number of VLs adsorbed on Cu(0 0 1) is shown in Fig. 4. In a fashion similar to the porphyrin molecules and to the SLs on metal surfaces, on Cu(1 0 0) each VL appears in STM images as four bright lobes arranged in a nearly rectangular configuration, generally with no contrast associated with the central board. ESQC calculations [28] confirm that, as for most molecules of the Lander family, only the legs or spacer groups of VLs are imaged by STM. From a qualitative point of view, the central board is too high above the surface for its molecular orbitals to have enough electronic coupling to result in a visible contribution to the STM image. When deposited at RT and without annealing, no long-range ordering of the molecules was observed. In many areas of the surface, the molecules are in direct contact, either with their long axis parallel to each other, forming short rows of molecules, or perpendicular to each other. In vacant spaces between molecules the tunneling current is very noisy, indicating that molecules are diffusing rapidly along the surface, either spontaneously or by being dragged by the STM tip. As a direct consequence, when imaging at RT it is generally not possible to retrieve the substrate surface corrugation between molecules.

Many molecules are imaged (Fig. 4, right hand panel) with large deviations from the "ideal" rectangular shape exhibited by the chemical structure. Moreover, some lobes in the images are characterized by a noticeable "shoulder-like" feature, as shown in the small insets of Fig. 4. These features indicate that the corresponding legs are sufficiently rotated relative to the perpendicular conformation from the original molecular design, leading to noticeable tunneling through their upper parts

as well as the usual tunneling through the lower parts. This is similar to previous results reported on porphyrin molecules [4,26].

Attempts to reproduce experimental images by ESQC simulations were successful only when the molecular geometry was effectively relaxed, allowing the σ bond attaching each leg to the board to be flexible. The conformation extracted by combining ESQC and MM2 shows that the legs are severely twisted, leading to a board–substrate distance much smaller than the one expected from the free-space chemical structure, which originally implied a rigid aromatic plane held apart from the surface by rigidly connected spacer groups. Most likely, the driving force for this molecular distortion is the van der Waals interaction between the molecule's π-system and the substrate.

More recently, Zambelli et al. [66] have studied by STM the adsorption of Double Lander (DL) molecules on Cu(0 0 1) and on a nanostructured Cu(1 1 1) surface. The DL has a 3.7 nm long conjugated board equipped with eight lateral legs for isolation from the substrate. The results indicate that not only the legs are free to rotate, but also that the central wire is distorted when adsorbed at the edge of Co/Cu(1 1 1) double steps. By detailed comparison with simulated ESQC images, it is concluded [66] that the van der Waals attractive interaction between the conjugated π-system and the underlying metal substrate is responsible for the observed deformation of DL molecules.

4. Manipulation experiments on metal surfaces

The controlled assembly of molecular arrays (supramolecular chemistry) requires atomic-scale positioning and interlocking of intact molecules, carefully avoiding a disruption of their internal structure. This possibility can be explored by using SPM, which combines high-resolution imaging for determining structure and orientation, and the capability of manipulating individual atoms and molecules, virtually at will. Presently scanning probes allow to perform engineering operations on the nanoscale, manipulating single atoms, molecules and bonds, and has thus become a tool that operates at the very limits of nanofabrication. Manipulations of individual entities on the nanoscale allow the building of predesigned supramolecular structures, the exploration of the influence of the chemical and geometrical environment on a particular molecule, or the development and testing of concepts for new nanodevices. Even though this is at present a serial approach and therefore, as such, unsuitable for direct practical applications, it has greatly enhanced our understanding of molecule–substrate and molecule–molecule interaction [67].

Generally speaking, manipulation experiments can involve the selective disruption of atomic bonds by means of voltage pulses, electric fields or mechanical contact between the probe's tip and the adsorbed entity. Controlled positioning of atoms and simple individual molecules (like CO) without rupture of intramolecular bonds was first achieved only at low temperatures [36,37]. Later it was extended to RT for single atoms [68].

A variation of the distance between the STM tip and the sample may be employed to exert a force on an atom or molecule adsorbed on a surface. A manipulation can be performed by lowering the tip towards the atom, thereby increasing the interaction between tip and atom or molecule. By adjusting tip position and reducing tunneling voltage, or increasing the tunneling current (or both), it is possible to adjust the magnitude and direction of the force, so that the tip can push or drag an atom or molecule across a surface, with the adsorbate still remaining bound to the surface [25,36–38,69,70]. After such an operation, the tip is withdrawn by resetting the tunneling voltage/current to the imaging values, and this effectively terminates the attractive interaction between molecules and tip. The lateral translation of atoms, clusters, and molecules is normally defined in terms of pulling, sliding or pushing, depending on the type of interaction that is used between tip apex and adsorbate (attractive for pulling and sliding, repulsive for pushing). While increasing the strength of the interaction by reducing the tip height, the manipulation mode changes from pulling to sliding. This occurs because the adsorbate is mainly following substrate minima in the case of weak tip–adsorbate interaction, exhibiting the discontinuities of adsorbate jumps. Normally lateral and vertical manipulation processes are employed for the manipulation of interestingly large molecules and clusters, in order to avoid their fragmentation.

During the manipulation process, changes in tunneling current indicate the distances between the adsorption sites adopted by the adsorbate. In general, the direction of motion of the atom or molecule on the substrate will depend on one hand on the shape of the molecule's and the tip's orbitals involved in the electrostatic (repulsive) interaction, and on the other hand on molecule–substrate interaction at various surface sites. This latter interaction in turn depends on the chemistry and the geometry of the chosen substrate.

4.1. Controlled positioning of Cu-TBPP on Cu(0 0 1) at room temperature

Operation at LT generally permits STM manipulation of weakly bound molecules with little or no contribution from thermal motion, therefore enhancing the ability to position molecules with atomic precision.

On the other hand, at RT it is important to have molecules that are strongly bound to the surface in order to prevent uncontrolled diffusion caused by the available thermal energy kT. Room temperature positioning of large molecules into predefined patterns and without disruption of internal molecular bonds is extremely important, because any realistic device must be able to operate at ambient conditions. It was first demonstrated by Jung et al. [25].

By evaluating several different molecules, Jung et al. [25] determined that Cu-TBPP meets the criteria necessary for precise positioning into predefined patterns, without disrupting its internal bonds. Due to a steric repulsion effect, on Cu(0 0 1) the molecule's four legs are rotated out of the plane of the porphyrin ring. In this case the *tert*-butyl groups dominate molecule–surface interactions.

In their manipulation experiments, Jung et al. [25] used a tunneling resistance of 10 MΩ, [1] which suggests a simple pushing mechanism. By analyzing molecular displacements, they conclude that tip–molecule repulsion is responsible for inducing translations. To illustrate this method, they first disrupt a molecular island consisting of a two by three array, by dragging the STM tip directly above it. Then individual molecules were displaced until a hexagonal ring was formed. Notably such rings do not form spontaneously upon annealing the Cu(0 0 1) substrate, which has a square lattice.

4.2. Manipulation in constant height mode: Cu-TBPP on Cu(1 1 1)

Lateral manipulation at constant current [69] is the technique developed to move atoms or small molecular adsorbates on metal surfaces by STM. In this case the STM tip is kept close to the surface by increasing the tunneling current (or decreasing the tunneling voltage, or both) and then moved laterally over the target atom or molecule. For example, at RT this method allows the displacement of single Cu-TBPP molecules on different Cu surfaces [25]. When operating at LT however, a much stronger repulsive force must be exerted for the interaction to be effective. In fact, at very low temperatures (below 20 K) on Cu(1 1 1) the application of the "standard" technique of lateral manipulation at constant current does not induce any movement of the molecule. The main problem of the constant current manipulation technique is that when the tip approaches the molecule, it is forced to retract as a consequence of its high conductance. Moreover, the feedback loop modifies the distance between tip and molecule to keep the current constant, and in the case of complex systems like Cu-TBPP, this may cause an instability of the tip position. As a consequence, the force applied by the tip cannot be controlled at will. To move Cu-TBPP molecules at LT it is therefore necessary to develop a new manipulation technique in order to apply a strong repulsive force and to keep the tip close enough to the molecule during the entire process.

For this purpose, a technique called "constant height manipulation mode" was recently developed by Moresco et al. [71]. To prepare for manipulation, the tip is initially moved back and forth between two points at either side of the molecule at constant current, allowing the measurement of the tip's height along the path. At this point, the feedback circuit is switched off and manipulation parameters are set. The tip then approaches the surface by a chosen distance Δz. Subsequently the tip moves across the molecule at constant height, and during this scan both the tip height and current signal are recorded. The current signal is important because it contains information on the dynamics of the manipulation process. Moresco et al. [71] successfully applied this technique to the Cu-TBPP on Cu(1 1 1) system.

Although on the Cu(0 0 1) surface Cu-TBPP is imaged as *four* bright lobes, on Cu(1 1 1) it appears in STM images as *eight* lobes, with an apparent height of only 2.2 Å per lobe [71] as shown in Fig. 5a. As was recently pointed out by Moresco et al.

[1] The tunneling resistance is defined as the ratio of the tunneling voltage and the tunneling current.

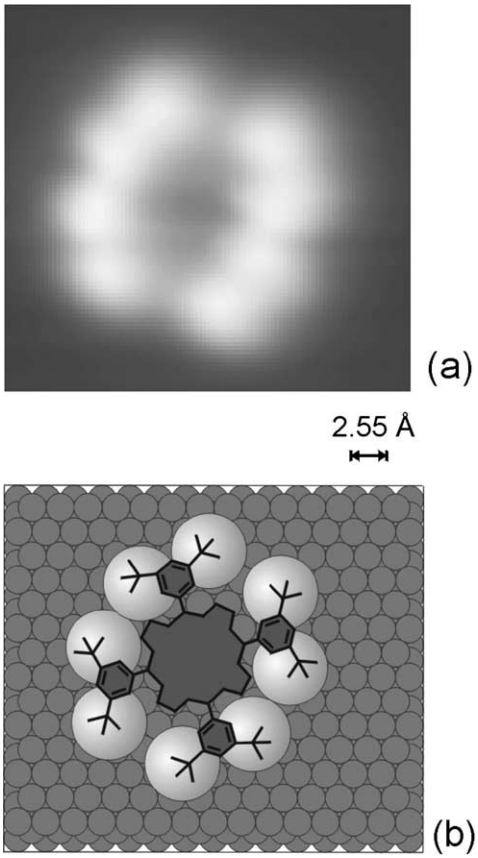

Fig. 5. (a) STM image of a Cu-TBPP molecule deposited on Cu(1 1 1). The image was taken at a tunneling current of 400 pA and a bias voltage of 300 mV. (b) Sphere model showing the orientation of the molecule on the Cu(1 1 1) surface. From Ref. [71], with permission.

[27], this striking difference is due to the different conformations adopted by the molecule on the two surfaces. By comparison with ESQC calculations, they deduce that these eight lobes simply correspond to the four legs lying flat on the surface. The legs are rotated parallel to the porphyrin plane, and the two external butyl groups of each leg interact with the surface, giving rise to exactly two lobes per leg, confirming what is observed in experimental STM images.

Overall, Moresco et al. [71] find that the manipulation signal shows several jumps of the molecule, not identical in form and length, as shown in Fig. 6. The behavior of the current is therefore more complex than expected from a simple translation, and can be described in terms of a superposition of the lateral displacement with a rotational movement. Other superimposed features are tentatively attributed to the molecule's internal degrees of freedom.

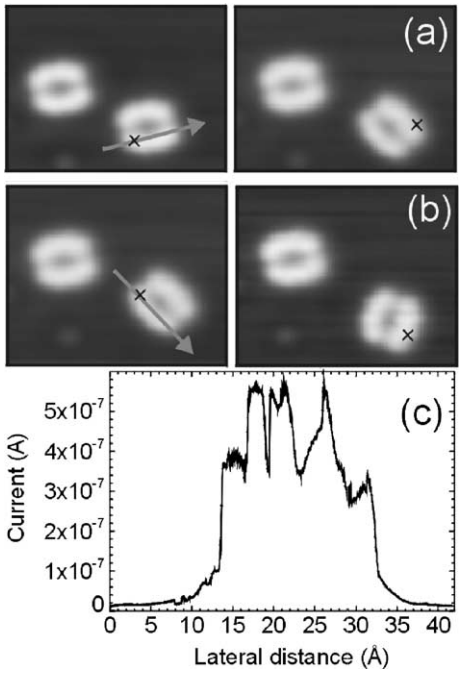

Fig. 6. (a and b) STM images showing the result of manipulation in the constant height mode, recorded at a tunneling current of 400 pA and a bias voltage of 300 mV. The images on the left indicate the position of the molecule before the process and the images on the right show the result of manipulation. The arrows indicate the path of the tip during manipulation. The tip interacts with the molecule through a single leg in the position labeled with an X. (c) Current signal recorded during manipulation in (b). From Ref. [71], with permission.

Normally, the manipulation signal yields details on the particular mode of manipulation, for example pushing or pulling. The information contained in a constant height manipulation signal is much richer and in principle contains information on intramolecular structure, intramolecular interaction and molecule–substrate interaction.

4.3. Conformational changes induced by STM manipulation: Cu-TBPP on Cu(2 1 1)

By an interplay of low temperature STM experiments and ESQC simulations, Moresco et al. [4] have recently demonstrated the ability of the STM tip to induce changes in the internal configuration of a large organic molecule, thereby modifying its electronic properties. The system chosen for this investigation was Cu-TBPP deposited on Cu(2 1 1). This substrate was chosen because it is characterized by a high density of steps. To implement this "molecular switch", vertical and lateral STM manipulation were employed to select and change the orientation of one Cu-TBPP leg, in a controlled manner. On this surface, although the force applied by the

tip is not strong enough to translate the molecule, it can induce the rotation of single legs in and out of the plane of the porphyrin ring. By measuring the current variation through the molecule's leg as a function of tip–molecule distance, they showed that this current depends strongly on the leg's orientation, which can be switched mechanically by the STM tip.

As in the case of Cu-TBPP on Cu(1 1 1) (just discussed in Section 4.2), on Cu(2 1 1) the legs lie nearly flat on the surface leading again to a total of eight lobes per molecule in STM images. This is caused by a strong interaction between the surface and the two end butyl groups of each leg.

By scanning over the molecule in lateral manipulation mode (with a tunneling resistance of 60 kΩ), a rotation of the legs out and/or in the porphyrin plane can be induced. As shown in the sequence in Fig. 7, where the manipulation was carried out in the direction of Cu(2 1 1) step edges through the legs, under these conditions a single leg can be rotated in both directions. The tilt from the rotated to the flat

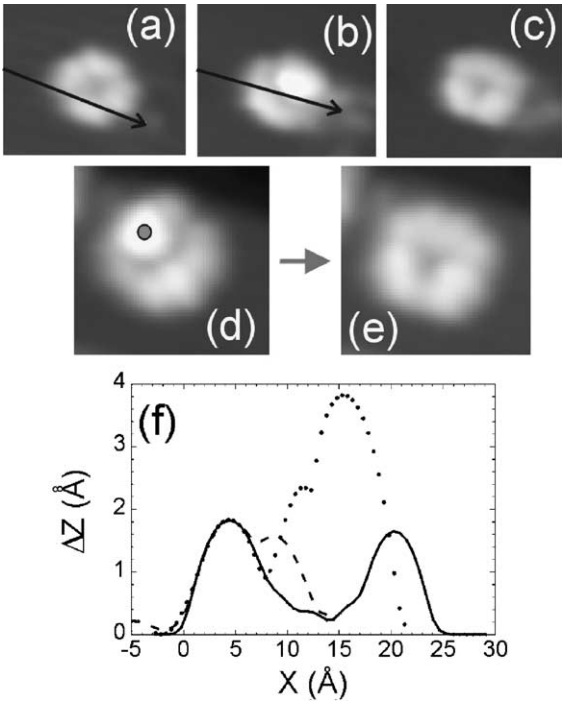

Fig. 7. STM images showing the rotation of a leg induced by (a)–(c) lateral and (d)–(e) vertical manipulation. The lateral manipulation was performed in the direction indicated by the arrows in (a) and (b) at a tunneling resistance of 6×10^4 Ω; (b) shows the result of the manipulation in (a), and (c) shows the result of the manipulation in (b). (e) Result of the vertical manipulation performed by positioning the tip on the point indicated with a circle on image (d). (f) Calculated STM scans of the Cu-TBPP molecule across an ON leg (dotted line), an OFF leg (dashed line), and across two opposite OFF legs (continuous line). From Ref. [4], with permission.

conformation corresponds to a transition between the ON and the OFF states of the switch. Moresco et al. [4] point out that this rotation can be obtained also by performing a vertical manipulation.

The principle of this molecular switch was demonstrated experimentally by studying the interaction between tip apex and leg during vertical manipulation. This was done by measuring the tunneling current as a function of the tip's height above the surface, as shown in Fig. 8. Not surprisingly, the switching process was found to be perfectly reversible.

Clearly this type of switch is far from being appropriate for practical applications, since it is too slow to be effective. Nevertheless it is very important as an exploratory device. Notably, it is more a mechanical switch than an electronic one. At the same time, it demonstrates the important concept of a macroscopic operator who is able to perform actions on the nanoscale, using an SPM tip as the appropriate interface.

4.4. Single molecule synthesis using the STM tip

As already mentioned, the STM has also been applied to induce simple chemical reactions on surfaces on the atomic scale [72]. Lauhon and Ho [73] for example were able to use the STM tip to break a C–H bond in a single acetylene molecule adsorbed on Cu(0 0 1) held at 9 K; they further proceeded to dehydrogenate the ethinil species to form dicarbon (CC) [73].

Besides the breaking of selected molecular bonds, the STM can also be used to induce a single bond formation. A good example of this process was reported by Lee and Ho [74], who were able to form Fe(CO) and $Fe(CO)_2$ molecules starting from Fe atoms and CO molecules adsorbed on Ag(1 1 0) held at 13 K.

More recently, Hla et al. [35] demonstrated the feasibility of inducing all the steps of a surface chemical reaction by using tunneling electrons from an STM tip. The concept of "Single molecule engineering" is illustrated in Fig. 9. Starting from iodobenzene adsorbed on a Cu(1 1 1) surface held at 20 K, they were able to synthesize biphenyl molecules, one at a time. The initial steps of this reaction are reported in Fig. 10 [35]: iodine is extracted from iodobenzene molecules using a voltage pulse from the tip, and a phenyl molecule is moved close to another phenyl molecule to prepare for association. Finally, the verification of successful chemical synthesis of two phenyls is shown in Fig. 11 [35].

The possibility of controlling chemistry at the spatial limit of individual atoms and molecules has provided new insights into the nature of chemical bonds and reactivity. For example, single molecule synthesis represents a way to study how the environment of the reactants affects surface reactions, or how the conformation of reactants affects reaction barriers.

Creating or synthesizing 'custom' made structures is perhaps one of the most exciting applications of manipulation. In this way it is possible to create totally new phases and structures of matter that are not normally accessible in nature. Once the new structures are fabricated, they can be investigated with the STM in the normal imaging and spectroscopy modes, and by other techniques. From a strictly practical point of view the main problem is the serial nature of manipulation techniques,

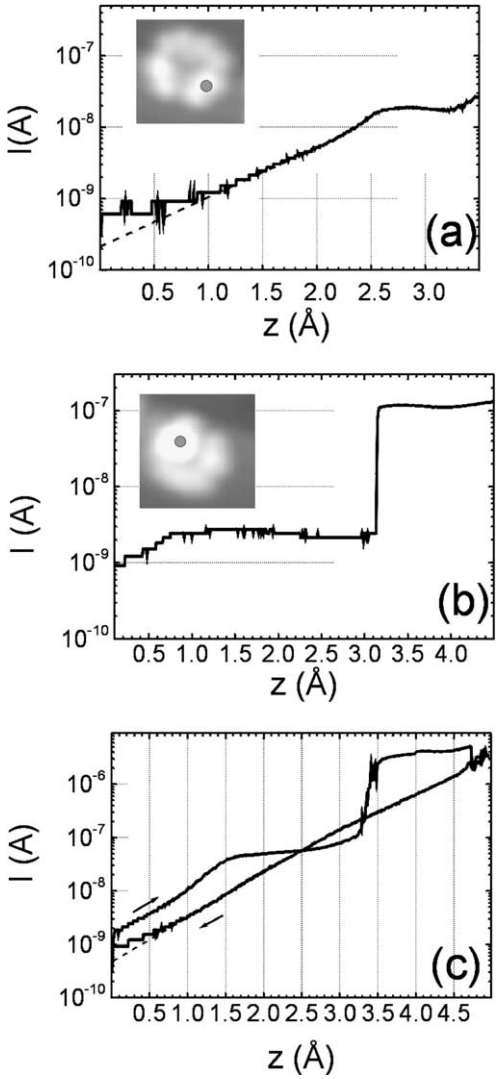

Fig. 8. $I(z)$ curves recorded (a) on an OFF leg and (b) on an ON leg. The exact position of the tip is shown in the insets. The starting tip–surface distance z_0 is, respectively, (a) 5.5 Å and (b) 7.5 Å, relative to the electrical contact point between tip and surface (12.7 kΩ STM junction resistance). (c) $I(z)$ curve recorded during the controlled rotation of a leg from the ON leg to the OFF leg states with $z_0 = 7$ Å. A sample voltage of 1 V has been applied during this $I(z)$ cycle. The dotted lines in (a) and (c) show the prolongation of the $I(z)$ behavior at low z, not visible in the experimental curves because of the limited sensitivity of the preamplifier. From Ref. [4], with permission.

versus parallel processes like optical lithography, which are much faster and therefore economically advantageous. Presently however, new atomic-scale structures are only accessible by means of manipulation experiments. Such structures often

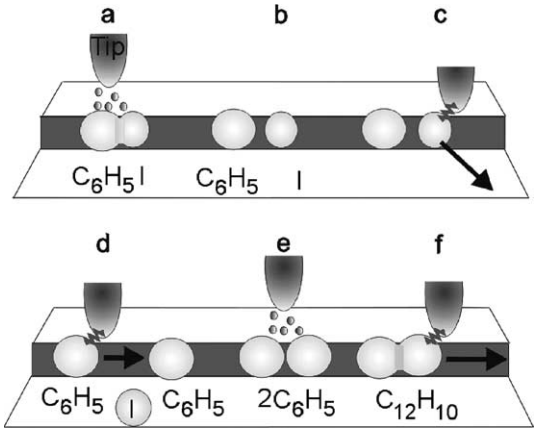

Fig. 9. Schematic illustration of the synthesis steps of a biphenyl molecule induced by the STM tip. (a and b) Electron-induced selective abstraction of iodine from iodobenzene. (c) Removal of the iodine atom to a terrace site by lateral manipulation. (d) Bringing together two phenyls by lateral manipulation. (e) Electron-induced chemical association of the phenyl couple to biphenyl. (f) Pulling the synthesized molecule by its front end with the STM tip to confirm the association. From Ref. [35], with permission.

represent model quantum systems, and therefore contain invaluable information on physical phenomena of fundamental importance.

5. Surface diffusion and rotation of large organic molecules on metal substrates

Surface diffusion of organic molecules is important both because of its fundamental scientific interest [75] and because of its role in the formation surface-bound nanostructures or in the growth of molecular thin films [76]. In general, knowledge of diffusion prefactors (these are D_0, h_0, defined below) contains precious information on film growth, and holds the promise of controlling growth properties.

Observation of adsorbate surface diffusion on the atomic scale has been reported in many cases by field ion microscopy (FIM) for metals on metals [77] and by STM for metal, semiconductor, or simple gaseous adatoms [43,78] on different substrates. By contrast, there are few contributions in the literature that report on the surface mobility of largish molecules [42,44,79].

In the simplest picture, a surface diffusion process can be viewed as a 2D random walk of an adsorbate, hopping with a rate h from adsorption site to adsorption site on the chosen substrate. A diffusion process is generally described in terms of three parameters. First, the activation energy for diffusion E_d is the barrier an adsorbate has to overcome on the potential energy surface to reach the at least the neighboring adsorption site. Second, the prefactor h_0 indicates the attempt frequency, i.e., the frequency with which the adsorbate in the potential of the adsorption site tries to overcome the barrier (the attempt frequency is roughly related to the adsorbates

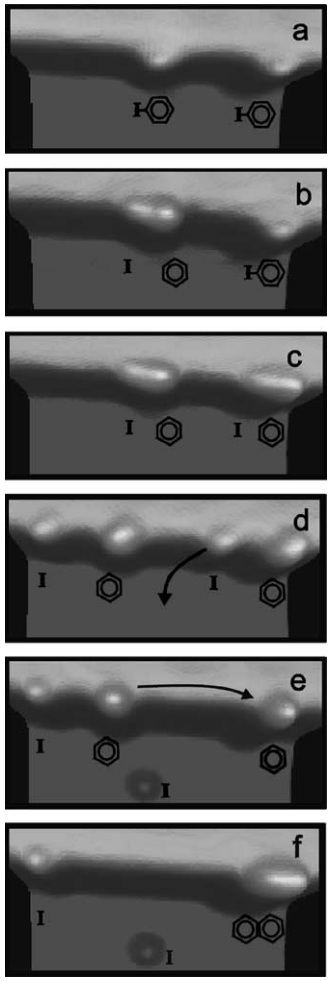

Fig. 10. STM images showing the initial steps of the tip-induced chemical synthesis. (a) Two iodobenzene molecules are adsorbed at a Cu(1 1 1) step edge. (b and c) Iodine is abstracted from both molecules using a voltage pulse. (d) Iodine atoms (small protrusions) and phenyl molecules (large) are further separated by lateral manipulation. (e) The iodine atom located between the two phenyls is removed onto the lower terrace to clear the path between the two phenyls. (f) The phenyl molecule at the left side is moved by the STM tip close to the right phenyl to prepare for their association. (Image parameters: $V_t = 100$ mV, $I_t = 0.53$ nA; 70×30 Å^2.) From Ref. [35], with permission.

lateral vibrational frequency). Finally, the root mean-squared (RMS) jump length λ contains information on the typical total distance jumped by the adsorbate. In the simplest case jumps are restricted between nearest neighbor (NN) adsorption sites only; however so-called long jumps, spanning multiple lattice spacings, are also possible.

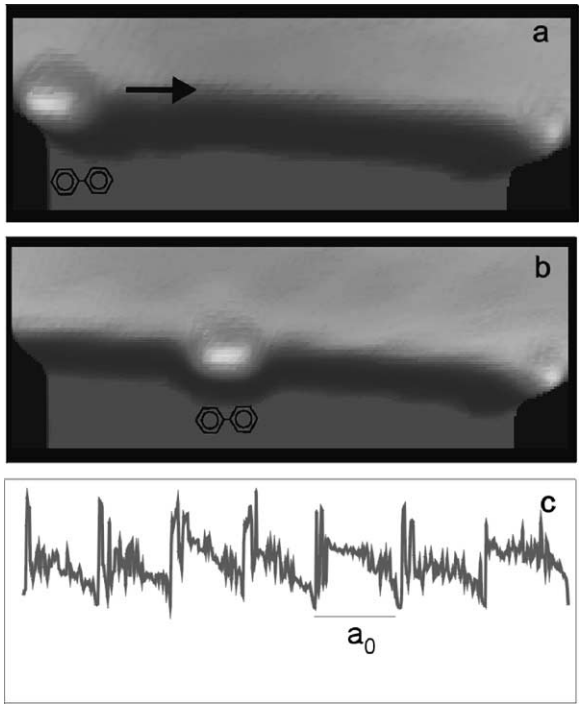

Fig. 11. Verification of successful chemical association of two phenyls. (a and b) The synthesized biphenyl molecule is pulled from the left part of the image to the middle by the STM tip. (c) The corresponding tip height curve reveals characteristic pulling behavior with the entire molecule trailing the STM tip for a distance of $7a_0$. (Image parameters: $V_t = 100$ mV, $I_t = 1.3$ nA; 60×20 Å^2.) From Ref. [35], with permission.

A quantitative analysis of diffusion data usually starts from an evaluation of the molecular displacements Δx along $[1\,\bar{1}\,0]$ between consecutive images, using a semi-automatic pattern-recognition routine [43] to identify which molecules have moved to which site. The molecular mean-squared displacement, $\langle(\Delta x)^2\rangle$, during the image acquisition time t, can be calculated directly from these displacement distributions and gives access to the hopping rate h to within a very good approximation [42].

The hopping rate h and the diffusion constant $D = \langle(\Delta x)^2\rangle/2t$ are often used to describe diffusion processes. Their temperature dependence is generally described by the Arrhenius law [75]:

$$h = h_0 \exp(-E_d/kT) \quad \text{and} \quad D = D_0 \exp(-E_d/kT) \tag{1}$$

where h_0 and D_0 are the hopping rate and diffusion constant prefactor, respectively, while k is Boltzmann's constant, and T the temperature. D and h are related through the fundamental relation [75]:

$$\langle(\Delta x)^2\rangle = \lambda^2 ht \tag{2}$$

The activation energy of diffusion E_d and the prefactors (h_0 and D_0) are typically extracted from a so-called Arrhenius plot ($\ln h$ or $\ln D$ versus $1/kT$).

A comprehensive review of adsorbate diffusion on metal surfaces was recently published [80], but it included few studies of large molecule diffusion on metals. In the following four subsections, we report on several STM studies of surface diffusion of large organic molecules on metallic substrates.

5.1. Comparative diffusion of DC and HtBDC on Cu(1 1 0)

In the present subsection we will compare the diffusion of decacyclene (DC, $C_{36}H_{18}$) and hexa-*tert*-butyl decacyclene (HtBDC, $C_{60}H_{66}$) molecules (shown in Fig. 12A and B, respectively in Ref. [42]) on a Cu(1 1 0) surface. We will indicate a new analysis method, used [42] to deduce the jump length in a simple way. This approach has led to new insight into surface diffusion processes. The two molecules described in the following consist of the same aromatic π-system, which adsorbs with its plane parallel to the Cu substrate. HtBDC has, additionally to DC, six *tert*-butyl groups surrounding the aromatic core [42].

The DC/HtBDC molecules were deposited in UHV from a resistively heated glass crucible onto an atomically clean Cu(1 1 0) surface. Molecular diffusion was studied by acquiring time-resolved STM movies with a variable-temperature STM [31]. For both molecules around 10 STM movies were recorded at specific temperatures in the interval 172–200/218–251 K for HtBDC/DC, respectively. Each movie was composed of 400–2500 image-to-image observations of individual, diffusing molecules, as exemplified in Fig. 12C and D (see also http://www.ifa.au.dk/camp/movies/ht79.mpg). For both DC and HtBDC, molecular diffusion was observed to be strongly one-dimensional, occurring parallel to the close-packed [1 $\bar{1}$ 0] direction of the Cu(1 1 0) substrate as indicated in Fig. 12C and D [42].

Arrhenius plots of h and D are shown in Fig. 13A for both DC and HtBDC. Activation energies and prefactors derived from these plots are 0.60 eV (HtBDC) and 0.72 eV (DC), with good agreement for both molecules. The lower activation

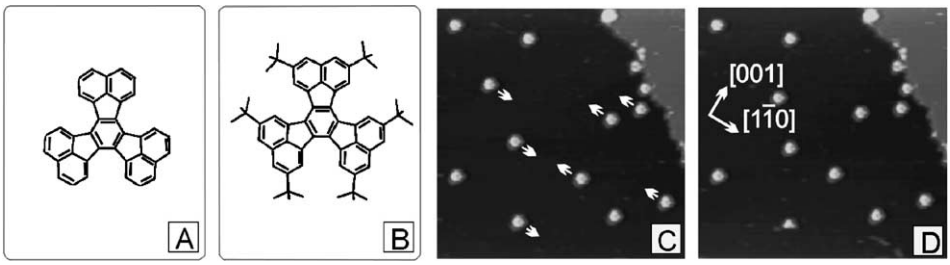

Fig. 12. (A and B) Chemical structure of DC and HtBDC, respectively. (C and D) Stills from a constant-current STM movie of HtBDC molecules, imaged as bright spots, on Cu(1 1 0) at $T = 194$ K ($V = 1768$ mV, $I = 20.61$ nA, 50×50 nm^2). Molecular displacements can clearly be discerned; arrows indicate the direction in which molecules will have moved in the successive image. From Ref. [42], with permission.

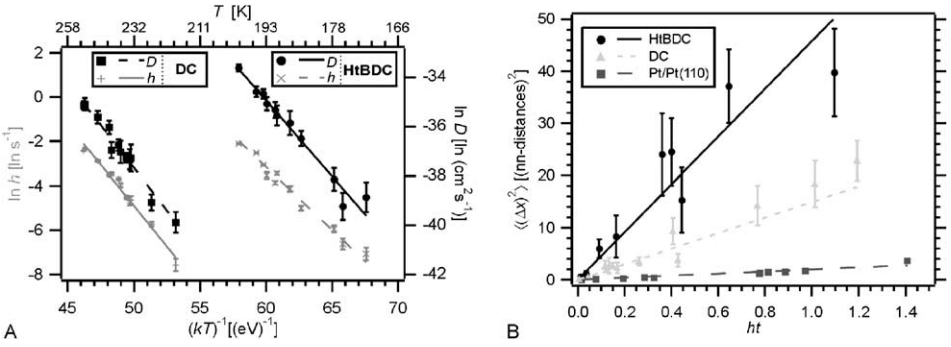

Fig. 13. (A) Arrhenius plots of the hopping rates h (gray) and the tracer diffusion constants D (black) for DC (left) and HtBDC (right). The lines are best fits to the Arrhenius expression for h and D (see Eq. (1)). (B) Plot of the mean-squared displacement $\langle(\Delta x)^2\rangle$ versus ht for HtBDC and DC. Also shown are data for diffusion of Pt on Pt(1 1 0) [43]. The lines are the best fits to Eq. (2) yielding the RMS jump lengths mentioned in the text. From Ref. [42], with permission.

barrier for diffusion of HtBDC compared to DC is attributed to the six *tert*-butyl spacer groups on HtBDC, which increase the distance between the surface and the aromatic π-system generally believed to interact strongly with the substrate. This leads to a diffusion constant that is four orders of magnitude higher than that of DC in the temperature range chosen for these studies [42].

The second part of this section deals with the problem of obtaining information on the jump length in surface diffusion processes. In the simplest picture, adsorbate migration occurs by random jumps between NN sites [42]. Although long jumps are also believed to contribute to the diffusion process in the case of weak adsorbate–substrate interaction, the experimental evidence for such events is still rather limited, being restricted in practice to the mobility of metal adatoms [43]. Attempts to extract information on jump lengths from diffusion constant prefactors were until recently hampered by large statistical uncertainties on quantities derived from Arrhenius analysis [81]. An alternative approach to distinguish contributions from double and triple jumps to metal-on-metal diffusion was introduced by Ehrlich and co-workers [82], and focuses on the entire atomic displacement distribution function. However, this approach is experimentally challenging, primarily because it requires a large, lattice-resolved data set for adatom diffusivity. Furthermore, the method is not suitable if there are large deviations from the simple single-jump diffusion picture.

Schunack et al. recently introduced a new, simple approach to determine root mean-square (RMS) jump lengths λ in surface diffusion [42]. Based on Eq. (2), they pointed out that the RMS jump length can be determined, provided that $\langle(\Delta x)^2\rangle$ and h can be obtained independently from STM images. Surprisingly, it was found that long jumps play a dominant role in the diffusion of these molecules [42]. From plots of $\langle(\Delta x)^2\rangle$ versus ht (see Fig. 13B) the RMS jump lengths are determined to be as large as $\lambda = 3.9 \pm 0.2$ and 6.8 ± 0.3 Cu NN distances for DC and HtBDC, respectively [42].

These findings are in strong contrast to the conventional NN hopping picture, which has been observed experimentally for metal-on-metal diffusion with values of λ close to unity in terms of NN distances [43]. With respect to atomic adsorbates, large molecules occupy a significantly larger area on the substrate of choice and therefore may find it more difficult to settle in a minimum of the potential energy surface. On the other hand, the longer jump length for HtBDC with respect to DC can be described in terms of its weaker interaction with the substrate, induced by the leg separation.

In conclusion, these results show the possibility of tailoring molecular diffusion properties: by raising the aromatic plane common to DC/HtBDC away from the surface by spacer groups in the case of HtBDC, this molecule has a diffusion constant which is approximately four orders of magnitude higher compared to that of its related molecule (DC) on the same surface. The higher diffusivity is due to a combination of larger RMS jump lengths and to a lower activation barrier for diffusion.

5.2. Diffusion of PVBA on Pd(1 1 0)

Surface diffusion of PVBA (4-*trans*-2-(pyrid-4-yl-vinyl) benzoic acid) on Pd(1 1 0) was reported by Weckesser et al. [79] based on STM studies. PVBA is an asymmetric molecule with a mass of 225 amu, and it consists of a pyridyl group attached to a benzoic acid via a vinyl group. Pd(1 1 0) is an fcc(1 1 0) surface, and it was chosen because of its anisotropy, which led to expect one-dimensional diffusion. Indeed STM observations confirmed that PVBA diffuses along the preferential [1 $\bar{1}$ 0] direction.

STM measurements were performed in the high tunneling resistance regime (>1 GΩ) to avoid any possible influence by the tip on the molecule's diffusivity. All attempts to manipulate PVBA molecules on this substrate were not successful, indicating a strong adsorbate–surface interaction.

STM images reveal that individual PVBA molecules lie flat on the surface and are imaged as protrusions with an apparent height of 1.25 Å and a length of about 11 Å. The shape found in the images is in accordance with the geometrical distance between the extremes of an isolated molecule. PVBA molecules are found to be randomly distributed on the surface, even upon post-deposition annealing, indicating that in this case molecule–substrate interactions greatly exceed molecule–molecule interactions. Analysis of STM images indicates that the molecules are bound to three neighboring Pd atomic rows, in agreement with STM observations on benzene/Pd(1 1 0) [83] and benzene/Ni(1 1 0) [84] where the C-ring was found at the fourfold hollow site of the substrate. The two different ends of the molecule do not exhibit different features in STM images. This is probably due to a transparency of carboxylic groups to tunneling electrons. The adsorption geometry reflects an optimal interaction between molecular subunits and the palladium surface, achievable without strong distortions of intramolecular or substrate structure. From a qualitative point of view, it is inferred that the surface chemical bond of PVBA with the Pd substrate is dominated by π binding through the electron ring systems of the pyridyl and benzyl groups.

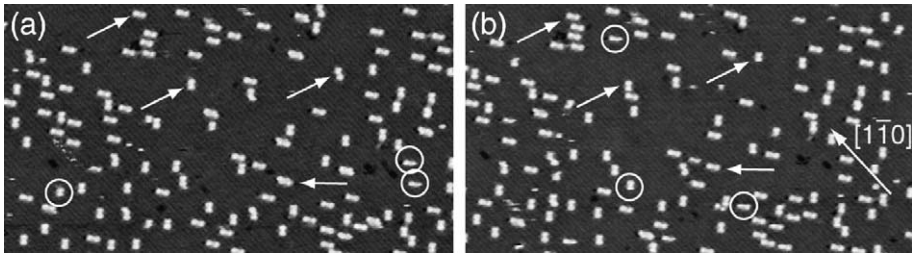

Fig. 14. STM images of PVBA on Pd(1 1 0). Two consecutive images show that individual molecules diffuse on the surface. From Ref. [79], with permission.

Surface diffusion of PVBA on Pd(1 1 0) was investigated in the temperature range 335–370 K. A comparison of consecutive STM images of the same area (with a time lapse of 220 s) clearly revealed that a fraction of the molecules changed position in the time interval between image recordings, as shown in Fig. 14. The analysis of positional changes between images showed unequivocally that PVBA surface diffusion is strictly one-dimensional along the close-packed substrate direction. This holds for higher temperatures due to the strong anisotropy of fcc(1 1 0) surfaces which results in different diffusivities along primitive surface directions.

By plotting the hopping rate versus $1/kT$ in Arrhenius fashion, the linear fit of the data yielded an activation energy for diffusion of 0.83 ± 0.03 eV and an attempt frequency $\nu_0 = 10^{10.3 \pm 0.4}$ s^{-1}. The activation barrier is quite high and indicates a rather strong bond between PVBA and the Pd substrate, as already observed qualitatively from the fact that manipulation attempts were not successful. On the other hand, the relatively small attempt frequency observed for this system may reflect a bonding configuration with reduced entropy in the transition state, leading to an effective reduction of the attempt frequency.

5.3. Diffusion of C_{60} on Pd(1 1 0)

Despite the large number of studies on the adsorption and growth of fullerene molecules on a great number of substrates, until recently [44] there was no detailed investigation of C_{60} surface diffusion.

Surface diffusion of C_{60} on Pd(1 1 0) by STM was reported in detail by Weckesser et al. [44]. Also in this case, the intuitive notion that the diffusion barrier would be smaller along the [1 $\bar{1}$ 0] direction than along [0 0 1] was confirmed by experimental observations. Diffusion rates for this system were determined in the temperature range 435–485 K. All attempts to manipulate the adsorbed molecules under various tunneling conditions were unsuccessful, again indicating strong molecule–surface interactions. The statistical hopping frequency was plotted versus $1/kT$ in Arrhenius fashion, and the linear fit led to an attempt frequency of $10^{14.4 \pm 0.4}$ s^{-1} and activation energy of 1.4 ± 0.2 eV along the close-packed direction.

The high value reported for the diffusion barrier probably indicates strong interactions and directional bonding between C_{60} carbon ring systems and Pd surface

atoms. Due to its size and round shape, C_{60} could well be a rolling buckyball, where high C–Pd coordination is retained, similar to the rolling motion of Ni clusters on Au(1 1 0) which were recently suggested in a theoretical study [85]. The large prefactors reported could be indicative of such a process, since a rolling motion would probably be characterized by a flat potential energy surface close to the transition state, which in turn can give rise to a high attempt frequency.

We note that the energy barrier is significantly lower for PVBA than for C_{60}. This is an indirect indication that binding is not restricted to the C atoms from C_{60} that are closest to the surface, i.e. a whole portion of each fullerene molecule is bound to the surface. At the same time, the attempt frequency is four orders of magnitude smaller for PVBA than for fullerene molecules. A plausible interpretation is that lateral interactions between PVBA molecules and the Pd surface are negligible, whereas the spherical shape of C_{60} leads to strong lateral π binding with Pd. Simpler molecules or atomic adsorbates diffuse like a "material point", with only one degree of freedom (translational). On the other hand, the lateral π binding of fullerene molecules can favor a rolling process. In conclusion, in terms of attempt frequency fullerene molecules seem to follow a more complex diffusion process than PVBA, with more than one degree of freedom (for example a rolling motion coupled to a translational one).

5.4. Discussion on surface diffusion of large molecules

In the two previous sections, we have illustrated and compared the surface diffusion of HtBDC and DC on Cu(1 1 0), and of PVBA and C_{60} on Pd(1 1 0). In the following section, we will attempt to draw analogies for the diffusion properties of all four molecules. Although the Pd(1 1 0) and Cu(1 1 0) surfaces are chemically very different, they are both anisotropic (with a preferential close-packed direction for diffusion), and they have the same geometrical structure.

In Table 1 below we recall and compare the activation energies and hopping rates and diffusion prefactors for the diffusion studies described in the previous sections.

We first compare the activation energies. From the values reported in Table 1 we notice that the activation energies of DC, HtBDC, and PVBA are comparable, being in the range 0.57–0.83 eV. The energy barrier for C_{60} on the other hand is about twice as large (1.4 eV). Since the activation energy is usually a fraction of the adsorption energy, this is an indication that fullerene molecules are more strongly

Table 1
Diffusion parameters (activation energy and attempt frequency) extracted from experimental surface diffusion studies of a few selected molecules (DC, HtBDC, C_{60}, PVBA) on two metal surfaces (Cu(1 1 0) and Pd(1 1 0))

	E_d (eV)	h_0 (s^{-1})
DC on Cu(1 1 0)	0.74 ± 0.03	$10^{13.9 \pm 0.7}$
HtBDC on Cu(1 1 0)	0.57 ± 0.02	$10^{13.5 \pm 0.4}$
PVBA on Pd(1 1 0)	0.83 ± 0.03	$10^{10.3 \pm 0.4}$
C_{60} on Pd(1 1 0)	1.40 ± 0.20	$10^{14.4 \pm 0.4}$

bound to the Pd surface than PVBA on the same surface and than DC and HtBDC on Cu(1 1 0). At the same time, we notice that the diffusion studies for PVBA and C_{60} were carried out at much higher temperature intervals, which is again an indication that surface binding of these molecules is stronger.

In terms of the attempt frequency, we note that it is four orders of magnitude smaller for PVBA than for C_{60} on the same surface, and for DC and HtBDC on Cu(1 1 0). This feature can be described in terms of the fact that lateral interactions between PVBA and Pd surface atoms are negligible, whereas they are strong for C_{60}. More generally, PVBA is likely to have a simpler diffusion behavior because of its size and shape, which would suggest diffusion properties similar to those of atoms or simple molecular adsorbates. The diffusive motion of HtBDC, DC, and C_{60} is most likely significantly more complex than for PVBA, since it could be coupled to a disk-like rotation (in the case of DC and HtBDC) or to a rolling motion (C_{60}).

5.5. Rotation of largish molecules on metal surfaces

The simplest version of a molecular "rotor" was first reported by Stipe et al. [86]. By applying voltage pulses by means of the STM tip, they were able to induce the rotation of single O_2 molecules on a Pt(1 1 1) surface. The rotation was then directly visualized by STM imaging. The process was found to be reversible among three different orientations on the chosen substrate (which has intrinsic threefold symmetry). Single-molecule rotational motion contains invaluable information on the molecular potential energy surface. The reversible rotation of a single diatomic molecule demonstrated by Stipe et al. is perhaps the simplest example of a memory or electromechanical device on the nanometer scale.

A more complex molecular rotor was observed by Gimzewski et al. [87]. By using STM at RT, they reported two spatially defined states of HtBDC on Cu(0 0 1), identified as immobilized and rotating, respectively. Similarly to the case of HtBDC on Cu(1 1 0), at submonolayer coverages the molecule exhibits extremely high mobility as a result of its weak adsorption to the surface. In this case there is a random array of voids in the supramolecular structure, where molecules are free to choose between different adsorption sites. In these voids, Gimzewski et al. [87] visualize individual molecules with the expected dimensions but in toroidal form instead of the usual six lobes, and consistently out of registry with the surrounding molecular lattice. This is an indication that, if enough space is available at sites of low symmetry, HtBDC molecules are able to rotate faster than the imaging speed. As a result the image is averaged over time, reducing the six lobes to the shape of a torus. The experimental results were supported by calculations of the rotational activation energy.

6. Molecule-induced surface restructuring

In the following sections, we present a few selected studies in which molecular overlayers or single molecules induced a local restructuring process on the metal substrate on which they were adsorbed. Similar phenomena were observed for

fullerene molecules on various metallic surfaces, and will be discussed in the next section, which deals with self-assembly of large organic molecules on metals.

More specifically, we will discuss STM results that directly prove that anchoring of complex molecules and the subsequent self-assembly of molecular nanostructures on a metal surface can be associated with a local disruption of the uppermost surface layer, just underneath the molecules. We will illustrate how a surface can undergo a restructuring process in order to accommodate specific molecular geometries [41,44–47], also leading to conformational changes within individual molecules [48]. Furthermore we will describe how a single fairly large molecule can act as a template on the nanometer scale, reshaping portions of a metallic step edge into characteristic nanostructures that are adapted to the dimensions of the molecule [41]. The restructured surface or step edge provides a preferential adsorption site to which the molecules are effectively anchored [41,45].

6.1. Interfacial roughening induced by phthalocyanine on Ag(1 1 0)

When deposited on Ag(1 1 0), Cu-phthalocyanine (CuPc) is observed to induce a transition [88] from mainly thermodynamically controlled 3D faceting at submonolayer coverage to a kinetically dominated, 2D step faceting process when coverage approaches a full monolayer. It was shown that same interaction mechanism that stabilizes new facets can also inhibit mass transport and prevent phase separation.

At submonolayer coverage (CuPc), induces faceting of slightly misoriented Ag(1 1 0) into three coexisting orientational phases. This orientational instability as observed by STM is caused by preferential adsorption of CuPc molecules at steps. On one hand, molecule–step interaction is sufficiently strong to stabilize new facets. On the other hand, it is weak enough to allow for mass transport on a mesoscopic scale, which is necessary for phase separation in large parts of the surface. Böhringer et al. [88] conclude that the observation of partially incomplete phase separation at submonolayer coverages indicates that 3D faceting would be inhibited for a slightly stronger molecule–step interaction. Furthermore, this shows that kinetic constraints can result in a drastically different surface morphology.

Surprisingly, deposition of a full monolayer gives rise to a very different surface morphology. The formation of a rigid molecular superstructure on (1 1 0) faces prevents large scale mass transport between terraces. The steps then relax to a more favorable orientation along molecular rows present on the (1 1 0) terraces.

6.2. Chiral restructuring imprinted by HtBDC on Cu(1 1 0)

The second example of this section describes the adsorption behavior of HtBDC on Cu(1 1 0) at elevated temperature, leading to a *surface restructuring process* which is actually *imprinted by the molecular overlayer*. Upon molecular deposition at RT, characteristic double row structures are observed with each HtBDC molecule being imaged as six lobes [45] (see Fig. 15A). The lobes are arranged in a distorted hexagon with threefold rotational symmetry and correspond to tunneling through

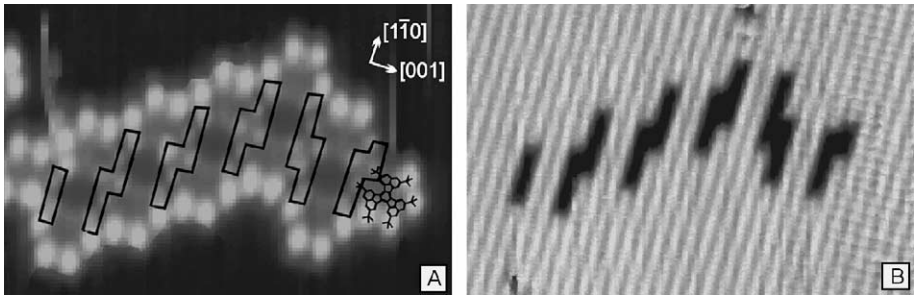

Fig. 15. Constant current image of HtBDC on Cu(1 1 0) at 41 K (10.5×6.9 nm^2). (A) HtBDC double row structure ($V_t = 1070$ mV, $I_t = 0.45$ nA). The trenches in the underlying surface are sketched in black and the chemical structure of a single HtBDC molecule is superimposed on the molecule to the very right. (B) Trenches in the surface layers are disclosed after displacing the molecules ($V_t = 7$ mV, $I_t = 1.82$ nA). The right part of the image shows atomic resolution along the close-packed direction (vertical-fast-scanning direction); resolution was abruptly lost when the tip scanned the restructured area. From Ref. [45], with permission.

the *tert*-butyl groups. Molecular rows run along two specific directions of the Cu surface and fluctuate in size, growing and shrinking from the ends. Moreover, at RT individual molecules diffuse rapidly between the double row structures on the surface [45]. All diffusive motion can be frozen out by cooling the sample below 150 K, as shown in Fig. 15A [45].

The STM tip was then used as a tool to manipulate the molecules within this double row structure. By scanning over the double row structure with reduced tunneling resistance, Schunack et al. [45] effectively displaced all adsorbed HtBDC molecules from a certain portion of the surface. A "clean" Cu surface area appears, as seen in Fig. 15B [45]. A local restructuring of the topmost Cu surface layer is directly revealed: 14 Cu vacancies are rearranged in two adjacent [1 $\bar{1}$ 0] rows, forming a trench-like base to which the molecules were anchored. From atomically resolved images where the molecular double rows and the Cu(1 1 0) lattice are resolved simultaneously, it is possible to determine the registry of the molecules. The three more dimly imaged *tert*-butyl lobes of each molecule are located on top of missing Cu atoms.

Upon closer inspection, it is apparent that the troughs are chiral [46]. In fact, it was found that at full coverage every molecule is associated with a chiral hole in the underlying surface. The observed molecule–hole complexes extend homogeneously over the entire surface and segregate spontaneously into enantiomorphic domains upon gentle annealing, thereby creating a perfectly ordered chiral metal surface.

The anchoring of molecules on the disrupted surface may have two causes. On one hand, it could be a simple steric effect, an adaptation of the surface geometry to allow the *tert*-butyl groups to fit into the trenches, resulting in a larger interaction area. Alternatively, the creation of steps and even kink sites underneath the molecules causes a higher reactivity of the substrate and therefore a stronger binding, since there is a simple correlation between the bonding strength of a molecule and

the metal coordination number of the adsorption site. Finally, it may also be a combination of these effects. Chirality induced by molecular overlayers will be further discussed in the next section on self-assembly.

If HtBDC molecules are deposited on the sample at temperatures below 250 K, the molecular double row structures do not form. Apparently at these temperatures there is not enough thermal energy available to promote adatom–vacancy formation and diffusion on Cu(1 1 0) [45,46].

These results show that the adsorption of large organic molecules on a metal surface can locally induce chirality on the underlying substrate. Since each molecule is associated with one kink site, it is inferred that the molecules are able to transfer a specific kink site chirality to the metallic substrate in a chiral imprinting process. This may ultimately lead to a new atomistic description of the asymmetric catalytic behavior of chirally modified surfaces.

6.3. Molecular molding at monoatomic step edges: Single Lander on Cu(1 1 0)

The Single Lander (SL) molecule was previously introduced in the earlier section (Section 3.2.1) on molecular wires. In the following section we describe its surprising property of acting as a molecular template on the nanometer scale, by means of a thermally activated process.

Upon submonolayer deposition of the Lander at RT, molecules adsorb on the surface and diffuse toward step edges, as shown in Fig. 16A (from Rosei et al. [41]). To investigate in detail the anchoring of the molecules on the surface, STM manipulation experiments were performed at LT on isolated molecules adsorbed on step edges that had been deposited at RT. By controlling precisely the tip's position, Rosei et al. [41] were able to selectively displace individual molecules one at a time along a predefined path, leaving the rest of the scan area unperturbed.

Surprisingly, such manipulation of individual molecules revealed an underlying restructuring of the monoatomic Cu steps induced by the docked molecules [41]. A manipulation sequence is shown in Fig. 16A–D, in which two neighboring molecules are removed from the step edge (neighbors in Fig. 16A and C). A peculiar metal nanostructure appears at the site where the molecules were previously attached (attachment sites in Fig. 16B and D); a zoom-in with atomic resolution is shown in Fig. 16E.

It is favorable for the Lander to anchor to the nanostructure at a step edge, because the gain in energy by adsorbing the molecule on this structure relative to its adsorption on a flat terrace is higher than the energy required for creating the structure. The dimensions of the molecules' board and legs fit in such a way that two rows of Cu atoms can be accommodated between the legs under the board. This leads to a favorable interaction between the π-system and the Cu atoms underneath. The dimensions and shape of the molecule form a perfect template for reshaping Cu kink atoms at the step edge, forming a nanostructure that is two Cu atoms wide and seven Cu atoms long. At step edges, Cu kink atoms are highly mobile at RT [89], but this mobility can be frozen out at LT.

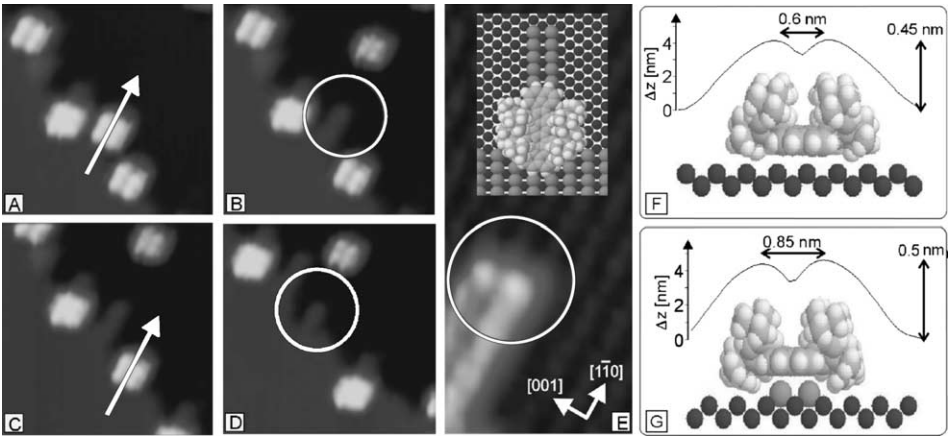

Fig. 16. (A–D) Manipulation sequence of the Lander molecules from a step edge on Cu(1 1 0). The arrows show which molecule is being pushed aside; the circles mark the tooth-like structures that are visible on the step where the molecule was docked. All image dimensions are 13 nm × 13 nm. Tunneling parameters for imaging are: $I_t = 20.47$ nA, $V_t = 21.77$ V; tunneling parameters for manipulation: $I_t = 21.05$ nA, $V_t = 255$ mV. (E) Zoom-in smooth-filtered STM image showing the characteristic two-row width of the tooth-like structure (right corner) after removal of a Single Lander molecule from the step edge. Cu rows are also visible. The inset shows the molecular structure, extracted from a comparison between experimental and calculated STM scans, demonstrating that the board is parallel to the nanostructure. The arrows show the directions on the surface. $I_t = 20.75$ nA; $V_t = 21.77$ V. Image dimensions are 5.5×2.5 nm^2. (F and G) Cross section of the nanostructure on a (flat) terrace and on step nanostructure and ESQC-calculated height profiles. From Ref. [41], with permission.

Height profiles measured across Lander molecules just before and after the manipulation sequences indicate that the molecules undergo a conformational change during manipulation. This shows that the interaction of the central board is optimized when the molecules rest on the nanostructure.

From ESQC calculations further insight was gained into the reason for these conformational changes (Fig. 16F and G). The molecular central board is strongly attracted to the surface because of the large π-system facing the metal substrate [41,42]. This introduces a severe constraint on the legs when the Lander lies on a flat terrace, which leads to an out-of-plane distortion of each leg-board σ bond. This σ bond almost restores its planarity relative to the board, because when the Lander is anchored to the structure, its central board is lifted up by more than 0.1 nm relative to the surface (Fig. 16F and G). This reduces the steric constraint existing on the leg-board σ bond, leading to an increased width (0.83 versus 0.63 nm) and height (0.50 versus 0.45 nm) of the Lander in the STM image, in good agreement with experimental results [28,41].

Upon adsorption of the molecules at LT (150 K), no restructuring of the Cu step edges is observed, and the molecules simply anchor to a step edge. At LT, the mobility of Cu kink atoms at the step edge is not high enough for the template to be effective. Thus Rosei et al. [41] concluded that this process is thermally activated.

In general, the intentional separation of a strongly bonding molecular subunit (such as the π-system in the Lander and in HtBDC) from a metal surface seems to be a driving force for a local restructuring of the metallic substrate, in order to regain an optimal interaction and adsorption geometry. This surprising property may prove to be important for designing molecules that could effectively engineer a surface in a predefined manner.

7. Self-assembly of large organic molecules on metal surfaces

So far, self-assembly appears to be one of the few practical strategies for fabricating ensembles of nanostructures in a parallel fashion. Since parallel processes are essential for industrial applications, it is expected that self-assembly will be an essential component of nanotechnology. In the present context, we limit the term "self-assembly" to processes that involve pre-existing components (distinct parts of an overall disordered structure), are reversible, and can be controlled to some extent by a proper design of the components.

Generally speaking, we can refer to self-assembly as "the autonomous organization of components into patterns or structures without human intervention" [90]. Self-assembling processes are common throughout natural phenomena and are often exploited in technological processes. Such processes involve components from the molecular (crystals) to the planetary (weather systems) scale and many different kinds of interactions. An alternative definition could be "the spontaneous formation of complex hierarchical structures from predesigned building blocks, typically involving multiple energy scales and multiple degrees of freedom" [91]. Self-assembled monolayers are therefore molecular assemblies that are spontaneously formed by adsorbing a specific molecule on a substrate.

Self-assembled organic thin films have a great number of practical applications, ranging from sensors [92] to heterogeneous catalysis [93], to biomaterial interfaces in medical implants [94], to the pharmaceutical industries. Polymorphism for example, which is the ability of a molecule to adopt different crystal forms, determines important physical and chemical properties of drugs, such as solubility and bioavailability. In general this characteristic is very difficult to control using standard growth procedures. It was recently shown [95] that the epitaxial growth of crystals onto organic single crystal substrates can influence growth morphologies, and this in turn can be exploited for controlling the resulting crystal structures by means of specific surfaces.

In this context, it is important to understand mechanisms that may induce self-assembly, and to describe at least qualitatively the forces that are responsible for these phenomena. Generally speaking, SAMs form as a result of a delicate balance between competing molecule–substrate and intermolecular interactions [96–101]. To control such processes in a useful way, it is therefore important to understand how this balance affects molecular nucleation and growth on a surface. The evolving adsorbate structures can be simple close-packed layers, or can exhibit more complicated patterns when directional bonds (for example hydrogen bonds [15,102] or electrostatic interactions [76,103]) are present.

In this review, we will only describe experiments in which SAMs were observed to form by OMBD of molecules in UHV ambient conditions.

7.1. Buckminster fullerene molecules (C_{60}) on metal surfaces

The first large organic molecule to be studied systematically on various substrates was C_{60}. Indeed the interaction between C_{60} and surfaces has attracted much interest since the discovery of fullerenes less than two decades ago. On metal surfaces, in particular, fullerene molecules exhibit a rich phenomenology. As will be described in the present section, upon adsorption they often induce a local restructuring of the substrate.

From a technological point of view, the substrate-induced modification of the electronic and structural properties of C_{60} is an important question to be addressed for possible future applications in molecular electronics [2,104] and molecular mechanics [105]. For example, Park et al. [105] reported the fabrication of single-molecule transistors based on individual fullerene molecules connected to gold electrodes. By performing transport measurements, they find evidence of a coupling—which appears in the form of nanomechanical oscillations—between the center of mass motion of C_{60} molecules and single-electron hopping. Transistors based on C_{60} molecules—which are compressed by the tip apex of an STM—or carbon nanotubes have been fabricated, and gain has been demonstrated in these devices.

From a fundamental point of view, the variety of bond strength and character observed in C_{60}–substrate interaction, ranging from weak van der Waals forces [106,107] to strong chemisorption [108], is atypical and still poorly understood. In particular, the growth of C_{60} on a multitude of different metal surfaces was studied intensively [19,20,49,109–112]. On most surfaces C_{60} tends to form well-ordered quasi-hexagonal close-packed overlayers with a nearest neighbor separation close to that of the van der Waals bonded C_{60} solid. On some substrates different C_{60} species were resolved by STM [113], but the cause of their different appearance has led to strong controversy. It is supposed to be either an electronic effect due to different orientations of the C_{60} cages or a geometric effect, due to a C_{60}-induced surface reconstruction. It could also be a combination of the two. As observed for Cu-TBPP, both surface chemistry and geometry play a significant role in determining molecular conformations and contrast in STM images.

Even for the most extensively studied system, i.e., C_{60} on Ag(0 0 1), this issue could not be resolved unambiguously [113,114]. In this case a dark and a bright C_{60} species can be observed by STM, and based on X-ray photoelectron diffraction (XPD) data Cepek et al. [114] identified the coexistence of two different C_{60} cage orientations. However, such orientations are not likely to be the origin of the contrast visible in STM images, which is probably related to orientationally ordered and disordered C_{60} cages. At the same time, strong substrate restructuring has been observed, for example for C_{60} on Ni(1 1 0) [20] and Au(1 1 0) [19], and it was recently reported that in the case of C_{60} deposited on Pd(1 1 0) the molecules reside on the 1×1 surface at intermediate temperatures, whereas they sink into substrate pits

upon thermal annealing of the substrate. This ultimately results in a much higher C–Pd coordination.

7.1.1. Adsorption of C_{60} on Au(1 1 0)

When adsorbed on atomically clean Au(1 1 0)–(1 × 2) surfaces, fullerene molecules induce significant mass transport of Au adatoms to form a (1 × 5) interfacial reconstruction [19]. STM images show that the underlying Au atomic arrangement is modified, maximizing the number of C_{60} molecules bonded to Au ridges in a distorted (6 × 5) hexagonal overlayer. Gimzewski et al. [19] concluded that the structure results from the balance between intermolecular van der Waals interactions, which favors the formation of hexagonal fullerene layers, and the strong C_{60}–Au interaction which favors bonding to the topmost Au atoms of [1 $\bar{1}$ 0] rows. The significant gold mass transport required is favored by the high mobility of Au surface atoms and by the small energy difference between the (1 × 2) and (1 × 3) Au missing row reconstructions.

In a more recent letter, Pedio et al. [111] reported surface X-ray diffraction measurements on the same system. Their data show that the C_{60}–Au interface is structurally more complex than the one previously inferred from STM images [19]. The early STM observations were partly confirmed by Pedio et al., since they indirectly observe that a large fraction of Au surface atoms are displaced from their original positions producing microscopic pits that may accommodate fullerene molecules. Moreover, they observed a p(6 × 5) superstructure in which the intermolecular distance between fullerene molecules is 10 Å, in agreement with the bulk C_{60}–C_{60} distance of 10.04 Å.

7.1.2. Comparison of C_{60} adsorption on Cu(1 1 0) and Ni(1 1 0)

The adsorption of fullerene molecules on the geometrically similar Cu and Ni(1 1 0) crystal surfaces was reported by Murray et al. [20]. Neither Cu(1 1 0) nor Ni(1 1 0) reconstruct in their clean state (as opposed to Au(1 1 0), which reconstructs 1 × 2). On Cu(1 1 0) the C_{60} hexagonal overlayer observed by LEED is directly confirmed by STM imaging. By contrast, atomically resolved STM images reveal that on Ni(1 1 0), the quasi-hexagonal diffraction pattern observed by LEED does not correspond to a simple overlayer structure. Instead it is found that C_{60} induces a restructuring process at the C_{60}–Ni(1 1 0) interface.

Fig. 17 reports an STM topograph that captures C_{60} in submonolayer quantity on Ni(1 1 0) ($T = 575$ K). The image shows that C_{60} molecules are aligned in one-dimensional rows along the [0 0 1] direction of the substrate, with adjacent rows varying in height. The vertical displacements between adjacent rows have height differences that are equal to the monoatomic Ni(1 1 0) step height. This height variation is observed to be independent of tunneling voltage and current [20] and is thus interpreted as a real topographic height. This rules out the possibility of the higher rows being a second C_{60} layer, since the C_{60} interlayer spacing should be almost one order of magnitude larger (7 Å). The corrugated structure described above is observed to be independent of C_{60} coverage, up to a full monolayer.

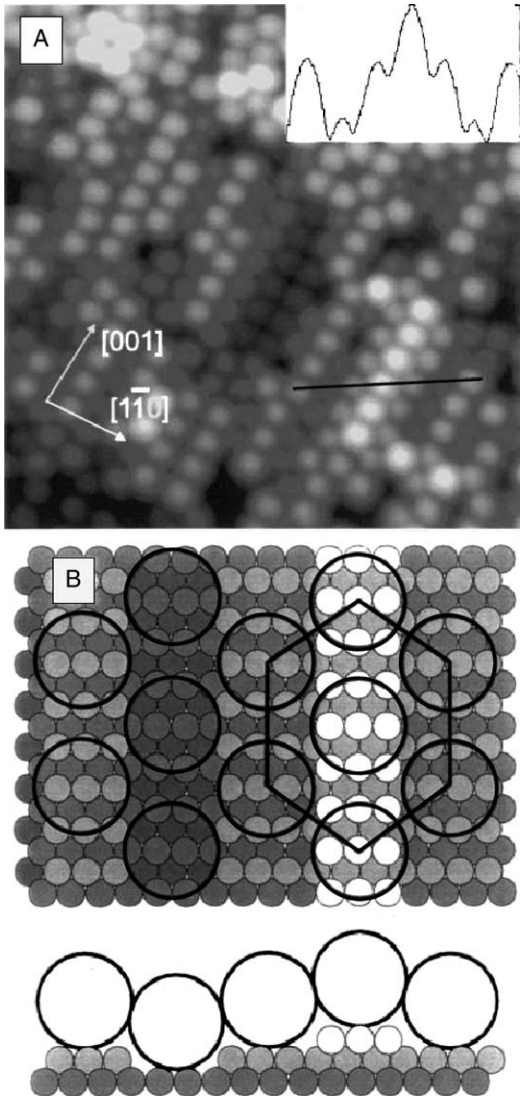

Fig. 17. (A) (Color) A 183×196 Å^2 image of C_{60} on Ni(1 1 0), corresponding to a saturation coverage, in which fullerenes are aligned in rows along the [0 0 1] direction of the substrate (labeled A). The hexagonal structure is outlined on the image. The inset shows a height profile taken along the line indicated on the image. (B) Schematic illustration of the structure observed in (A). The formation of added/missing [0 0 1] rows of Ni atoms creates the corrugated structure resulting in the formation of (1 0 0) facets and an increase in the C_{60}–Ni coordination. From Ref. [20], with permission.

The features observed on Ni(1 1 0) can be described in terms of interfacial roughening or even restructuring of the substrate via the addition/removal of Ni[0 0 1] rows as illustrated in Fig. 17B. This reconstruction results in the creation of

(1 0 0) Ni microfacets, rather than the expected (1 1 1) microfacets that stabilize many reconstructions of the open (1 1 0) fcc surfaces. This faceting process subsequently increases C_{60} coordination to the Ni substrate between rows of varying height. STM images also suggest that the mass transport involved in the restructuring occurs on a local scale, with Ni atoms squeezed from the terraces locally forming adjacent added rows.

The surprising difference between Cu and Ni surfaces was described in terms of a simple model, based on the interaction between the molecular orbitals of C_{60} and the narrow d bands of the surface. In general, for a restructuring or interfacial roughening to occur on a metal surface, the gain in binding energy must compensate for the energy cost involved in disrupting metal bonds. Metal atoms of the late transition series with a low coordination number have d states that are shifted up in energy relative to states for atoms with a high coordination number [115]. The upward shift of the metal d states makes the bonding of C_{60} sufficiently large to compensate for the energy cost in restructuring the surface. This effect is stronger on Ni(1 1 0) than on Cu(1 1 0), since for Cu(1 1 0) the separation between the d band and the C_{60} LUMO state is larger.

7.1.3. Adsorption of C_{60} on Pd(1 1 0)

A comprehensive study on the binding and ordering of C_{60} on Pd(1 1 0) was recently reported by Weckesser et al. [47], by combining several complementary surface-sensitive techniques: STM, LEED, XPS, and XPD. It was found that the rearrangement of Pd substrate atoms plays a crucial role in the evolution of C_{60} thin films.

Fullerene molecules were adsorbed on atomically clean Pd(1 1 0) surfaces held at RT. Deposition was followed by a high-temperature annealing cycle (usually 700 K). Evaporation of C_{60} on a Pd(1 1 0) surface held at the respective high temperature was found to yield equivalent structures. For this system, elevated temperatures are necessary to produce well-ordered structures. At low coverages (up to about 0.2 ML) fullerene molecules are arranged in stripes with a preferential width of two molecules, with an orientation roughly perpendicular to the close-packed Pd rows. On flat terraces, Pd islands are observed (with the same height of 1.4 Å as for monatomic steps on this surface), which are edged by C_{60} clusters. This implies strong lateral C_{60}–Pd interactions, since Pd islands on flat terraces are never observed on the clean surface. Pd island formation reflects the presence of mobile Pd adatoms in the terraces at elevated temperatures, similarly to the case of diffusing adatoms and vacancies on Cu(1 1 0). During cooling to RT, fullerene molecules are observed to aggregate into clusters, simultaneously trapping metal adatoms. The apparent imaging height of C_{60} molecules (3.1 ± 0.2) Å is much lower than expected from their hard-sphere diameter (7.1 Å). This imaging height is therefore thought to indicate a substrate restructuring process [44], in which fullerene molecules drive the formation of microscopic pits. Such pits or vacancies are two Pd layers deep and oriented along the close-packed [1 $\bar{1}$ 0] direction. By contrast, when depositing at temperatures below 500 K, isolated fullerene molecules are bound to the Pd surface and typically appear as 5.5 Å high protrusions. This surface restructuring process seems to be local

as in the similar cases of C_{60} on Au and Ni single crystals with (1 1 0) orientation, also resembling somehow what was observed for HtBDC and Lander molecules on Cu(1 1 0).

At higher coverage, the striped phase along $[1\,\bar{1}\,0]$ almost covers the whole substrate [47]. By annealing to 970 K an ordered phase of alternating bright and two dark rows along $[1\,\bar{1}\,0]$ extends over the entire surface. This single domain structure is referred to as the triple-stripe phase. Another well-ordered phase extending over the whole surface is found when further increasing the coverage. This phase simply consists of alternating dark and bright rows, and is referred to as the rotated-stripe phase. Overall on Pd(1 1 0) three distinct fullerene species are observed, characterized by different apparent heights with respect to the surface (3.1 ± 0.2), (4.6 ± 0.2), and (5.5 ± 0.2), respectively.

Molecular orientation of adsorbed fullerene layers was determined with high precision by measuring XPD patterns, which represent a real-space fingerprint of molecular orientation. For this system, XPD analysis shows that there is a unique C_{60} cage orientation.

Overall, three ordered structures evolving at elevated temperatures were identified, with significantly different unit cells $\left(\begin{pmatrix} 7 & -1 \\ \mp 2 & \pm 5 \end{pmatrix}, (4 \times 5), \text{and } (4 \times 8), \text{corresponding to coverages of 1, 0.82, and 0.77 ML, respectively}\right)$. A comparison of LEED and XPD results completes the understanding of the film structure, revealing that a substrate reconstruction is encountered with all three regular phases. Each structure has a unique orientation of C_{60} cages, by which the molecules are oriented with a bond between a five- and six-membered ring towards the substrate.

7.2. Comparative adsorption of HtBDC and DC overlayers on Cu(1 1 0)

As mentioned before, HtBDC is a prototype in the area of molecular electronics, designed for example to act as a molecular wire by means of its central aromatic π board, which is lifted from the surface by appropriately designed spacer groups. DC is very similar to HtBDC, except that it lacks the six additional *tert*-butyl spacer groups around the common central aromatic structure. By comparing the interaction of DC and HtBDC with Cu(1 1 0) it is therefore possible to study the interesting effect of separating/not separating the conducting parts of the molecule from the substrate. This has direct implications on the diffusion properties, as discussed earlier, and on the bonding and ordering behavior, as will be described in the following. Neither DC nor HtBDC possess molecular functionalities that may give rise to directional (strong) intermolecular interactions, and therefore intermolecular forces in this case are reduced to weak van der Waals interactions.

In Fig. 18 we show the growth of HtBDC layers on Cu(1 1 0) at increasing coverage. Molecular rows grow in length and density with increasing coverage, and characteristic "zigzag" rows, which alternate irregularly along the $[\bar{1}\,1\,\bar{2}]$ and $[1\,1\,\bar{2}]$ directions, eventually cover the entire surface (Fig. 18). If this disordered saturated overlayer is annealed at 410 K for around 10 min, uniform domains with diameters in the range of 100–1000 Å are formed. Each of these domains consists exclusively of

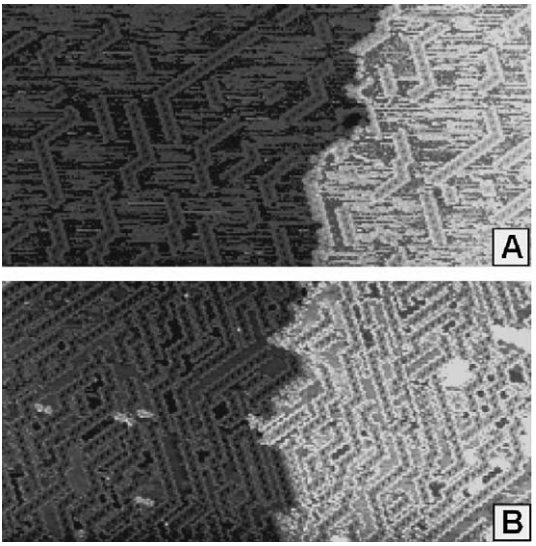

Fig. 18. Constant current STM images at RT displaying increasing coverages of zigzagged HtBDC rows (1000×500 Å^2, $V_t = 1250$ mV, $I_t = 0.55$ nA). (A) About 0.01 ML. (B) About 0.03 ML. From Ref. [46], with permission.

densely packed rows along the $[\bar{1}\,1\,\bar{2}]$ or $[1\,1\,\bar{2}]$ directions (Fig. 19). From the unique correlation between row direction and hole type underneath (cf. with Section 6.2), it is inferred [46] that holes within a given domain are all alike and hence the domains are homochiral, where every molecule is connected with a chiral kink site. This occurrence shows how the molecules induce chirality to the extended terraces of the metal crystal surface. Complementary results were reported by Lorenzo et al. [93], who observed that extended supramolecular assemblies of (R,R)-tartaric acid adsorbed on Cu(1 1 0) destroy existing symmetry elements and directly imprint chirality to the modified surface.

In a subsequent experiment, Schunack et al. [116] studied the adsorption of DC molecules on atomically clean Cu(1 1 0) surfaces, from the early stages of growth to the formation of a full layer. Perhaps not surprisingly, they found that DC occupies specific adsorption sites on Cu(1 1 0) in the same way as HtBDC does with the expected planar adsorption, which causes a strong interaction between the aromatic π-system and the Cu substrate. Even though the internal molecular structure as seen in STM images is much less pronounced for DC than for HtBDC (which was dominated by the *tert*-butyl appendages), two equivalent molecular conformations were found for DC, which can be overlapped by mirroring DC molecules across a $(1\,\bar{1}\,0)$ plane.

Unlike HtBDC molecules, DC molecules do not preferentially decorate step edges (Fig. 20) [116]. This may be described in terms of the strong, direct interaction of the aromatic core with the substrate, which reduces its mobility compared to HtBDC. A further difference compared with HtBDC is that, at low coverages, DC shows no

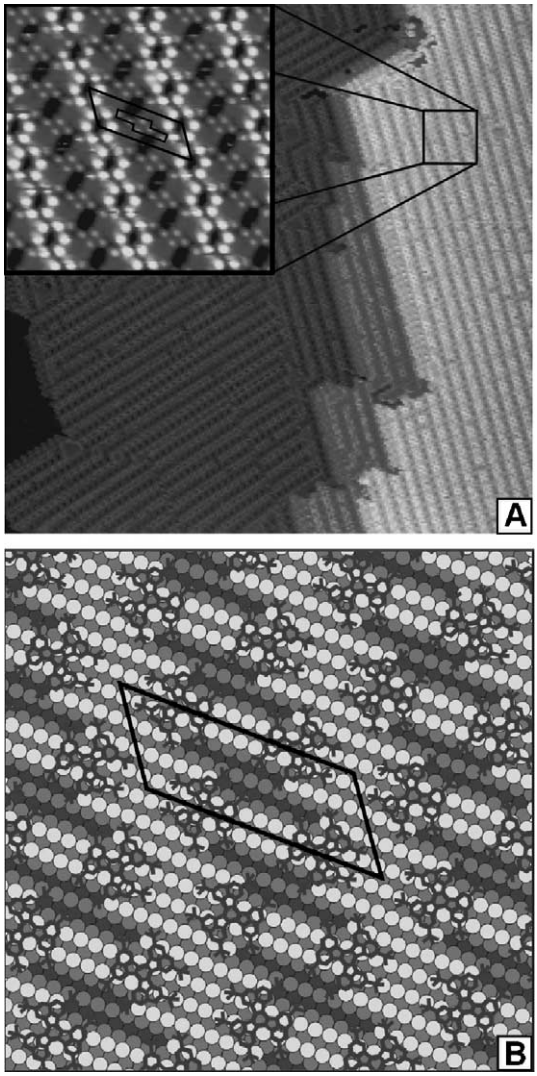

Fig. 19. Constant-current STM image at RT after annealing the fully covered surface (see Fig. 18B) at 410 K. (A) Domains of densely packed molecules along the $[\bar{1}\,1\,\bar{2}]$ and $[1\,1\,\bar{2}]$ directions (1000×1000 Å^2, $V_t = 1250$ mV, $I_t = 0.51$ nA). The inset shows a close-up of a domain (100×100 Å^2, $V_t = 1768$ mV, $I_t = 0.30$ nA): the characteristic unit cell and the hole contour are framed black. (B) Ball model of the double row structure—the substrate atoms are shaded darker whenever the layers lie deeper. The molecules are shown in red and the unit cell is framed black. From Ref. [46], with permission.

tendency to form clusters, probably because of the lack of directional, intermolecular forces. This represents a pronounced difference from the HtBDC case [45,46]. There the separation of the π-system from the surface in the case of HtBDC causes the

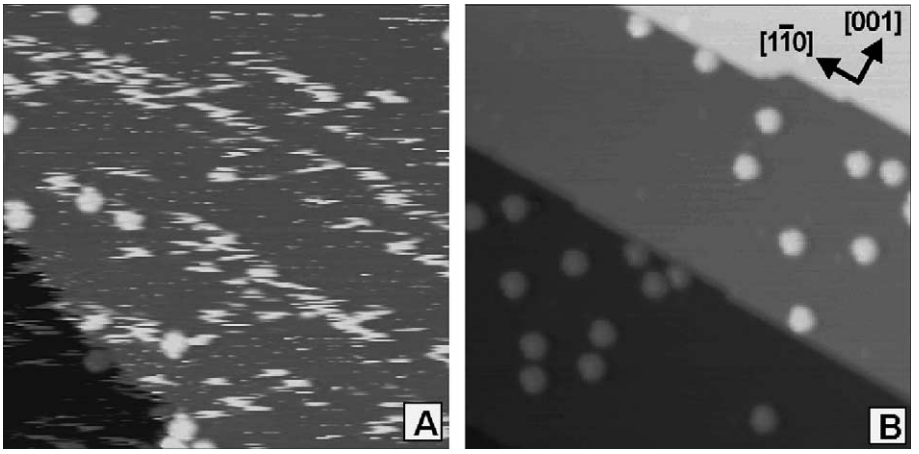

Fig. 20. Constant-current STM images of DC on Cu(1 1 0) at low coverages (300×300 Å^2, deposition time: 1 min). (A) At RT only few molecules are imaged. The streaks run preferentially along the close-packed Cu direction, indicating fast molecule diffusion ($V = -884$ mV, $I = -0.35$ nA). The Cu step appears fringed due to the high mobility of Cu kink atoms. (B) At 96 K diffusion is frozen out and single molecules are visible ($V = -1250$ mV, $I = -0.34$ nA). Also Cu kink atom mobility is reduced and the steps are stable with single kinks visible. From Ref. [116], with permission.

chiral surface restructuring which is eventually responsible for the formation of ordered HtBDC double rows.

By carrying out STM manipulation experiments, Schunack et al. [116] observe that, despite their similarity with HtBDC molecules, DC molecules do not induce a restructuring process within the topmost Cu surface layer. In this case a possible gain in adsorption energy on the restructured surface cannot compensate for the energy required to rearrange the Cu substrate [45]. Indeed, all the differences in the adsorption behavior of DC compared to HtBDC and other related molecules [41,45,48] can be described in terms of the variation of molecule–substrate interaction caused by the absence/presence of spacer groups. This again points to the possibility of appropriately designing molecules to tailor their properties, enabling them for example to restructure a surface in a predefined manner. Alternatively, predesigned molecules could be used to imprint specific patterns that may be used as templates for further growth.

When molecular coverage is increased it is observed that the density of fully imaged DC molecules increases. However, there seems to be no tendency to form ordered domains even at coverages close to a full monolayer, and even when annealing the deposited molecular overlayer up to 700 K. Because of the absence of attractive intermolecular forces in this case, molecular coverage is not high enough to force the molecules into an ordered arrangement.

Pronounced long-range order is only observed if the molecules are deposited over a longer period of time onto a heated Cu surface (450 K). Different types of domains can be observed as seen in Fig. 21A, and the ordering can be described in terms of a

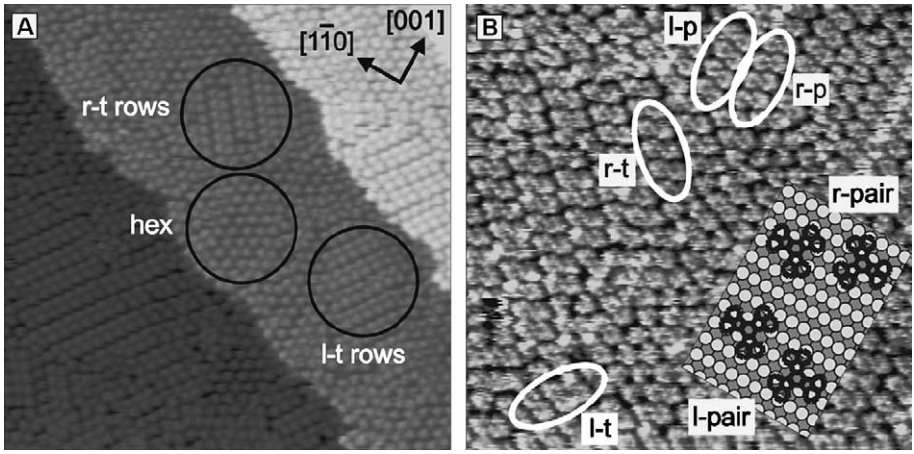

Fig. 21. Ordered phases of DC molecules appear on the surface after a deposition time of 15 min at elevated sample temperatures (450 K). The images are acquired at RT. (A) Three types of domains appear and are marked by circles: striped domains consisting of double rows of molecules (denoted "r–t" and "l–t") and quasi-hexagonal domains (500×500 Å^2, $V = -1768$ mV, $I = -0.43$ nA). (B) Mixture of different domains resulting from l- and r-pairs (see model inset) of DC molecules (300×300 Å^2, $V = -526$ mV, $I = -0.33$ nA). Four kinds of row structures can be formed out of these: l-p, r-p, r-t, and l-t. From Ref. [116], with permission.

simple model based on a molecular close packing on the substrate. Common structural elements in these domains are pairs of DC molecules along the $[1\,\bar{1}\,0]$ direction (Fig. 21B) which are simply the result of close packing at high coverages. These enantiomorph pairs are the basic building blocks in terms of which the dense packing into enantiomorph domains can be described.

The structures observed are simply close-packed domains that can be viewed as a repeated arrangement of molecule pairs. Such domain structures can be understood by assuming well-determined, identical adsorption sites of the DC molecule on the substrate. The molecules are then arranged in a way that minimizes the repulsive interactions between them, since only weak van der Waals forces are apparently active between DC molecules. In this respect the structure formation is also ruled by dominating molecule–substrate interactions as in the case of HtBDC molecules.

7.3. Self-assembly of PVBA on Ag(1 1 1) by hydrogen bonding

Among supramolecular structures formed by self-assembly, particularly interesting are those driven by hydrogen bonding, which provides both high selectivity and directionality [117]. Complex architectures involving hydrogen bonds are abundant in biological systems, and this has motivated their use in supramolecular chemistry [118].

Barth et al. [15] have recently shown how novel supramolecular nanostructures can be generated at surfaces by means of hydrogen bonding. By using STM, they characterized the adsorption of PVBA on a silver surface, observing that a one-dimensional supramolecular nanograting can be fabricated on Ag(1 1 1) by a cooperative self-assembly process.

In Section 5.2 we described the diffusivity of PVBA on a Pd(1 1 0) substrate. This molecule was specifically designed to form strong hydrogen bonds, and has been used to grow thin films for applications in non-linear optics [119,120].

Upon adsorption, the molecules experience the potential energy surface of the metal substrate of choice, and as previously described, this leads to specific geometries that are energetically more favorable. Once again, surface mobility, the competition between intermolecular interactions and molecule–substrate interactions, and thermal energy are the key parameters that govern the level of ordering that can be achieved in arranging molecules at surfaces. The balance of these factors is ultimately responsible for molecular self-assembly.

STM topographies reveal that on Ag(1 1 1) flat adsorption of PVBA prevails. On this substrate, formation of molecular islands is found even at LT. The island shapes indicate that their formation is a result of attractive interactions between molecular end groups. This observation is consistent with the directional interactions expected from the formation of hydrogen bonds.

Molecular strings are therefore able to evolve on this surface, and their curved shape implies that the substrate corrugation experienced by the molecules must be rather weak. This effect is attributed to the smoothness of the close-packed geometry of the substrate and the overall weak bonding between the adsorbate and the noble metal surface. The growth process reported by Barth et al. [15] can be considered as a diffusion-limited aggregation of rod-like particles, which is subject to anisotropic interactions. Accordingly, the irregularity of the formed agglomerates suggests that their shape results from kinetic limitations, which prevent from reaching thermal equilibrium.

The images reported in Fig. 22 show that well-ordered supramolecular structures evolve on Ag(1 1 1) when the thermal energy is increased by adsorption or annealing at 300 K. In particular, Fig. 22a reveals the formation of highly regular, one-dimensional supramolecular arrangements in a domain that extends over two neighboring terraces that are separated by an atomic step. Three rotational domains of this structure are found, in agreement with the threefold symmetry of Ag(1 1 1). A close-up view of some molecular stripes (Fig. 22b) reveals that the one-dimensional superstructure actually consists of two chains of PVBA. The molecular axis is oriented along the chain direction, consistently with the expected formation of hydrogen bonds between PVBA end groups. A closer inspection reveals that the molecules in adjacent rows exhibit antiparallel alignment. This is another example in which the geometrical arrangement of the molecules is a compromise between the lateral intermolecular interaction and the bonding to the substrate.

This regular mesoscopic ordering of the supramolecular chains into a grating is somewhat reminiscent of mesoscopic superstructures induced by relaxation of sur-

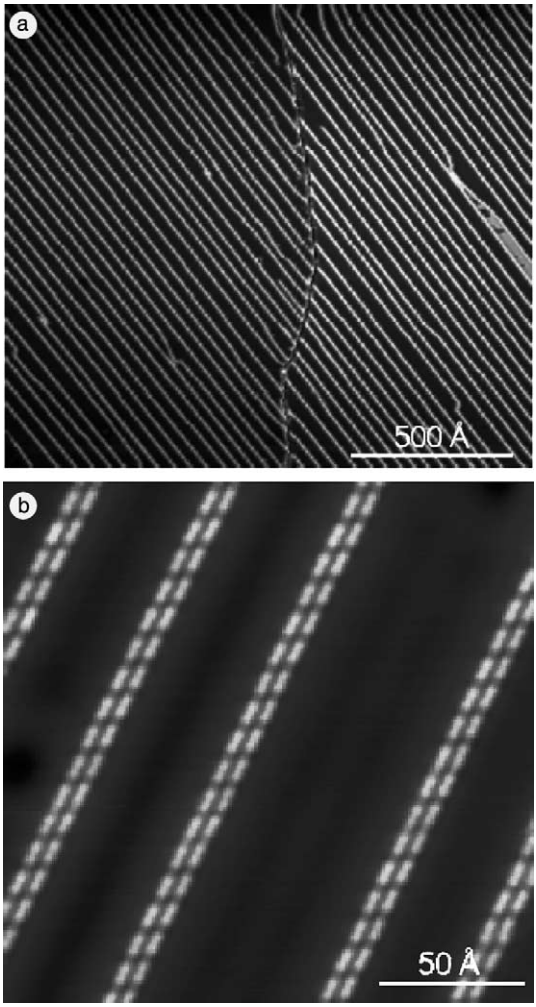

Fig. 22. Formation of a one-dimensional supramolecular PVBA superstructure by self-assembly mediated by H-bond formation on an Ag(1 1 1) surface at 300 K (measured at 77 K). (a) STM topography of a single domain extending over two terraces demonstrates ordering at the mm scale. (b) Close-up image of the self-assembled twin chains reveals that they consist of coupled rows of PVBA molecules. From Ref. [15], with permission.

face strain [121,122]. In this sense, it can be tentatively described in terms of weak, long-range repulsive dipole–dipole interactions between twin chains [123].

The work reported by Barth et al. [15] suggests that self-assembly of properly designed molecules by non-covalent bonding opens new possibilities for positioning functional units in supramolecular architectures on metallic substrates by OMBD. This approach may become useful for fabricating nanoscale devices and supramolecular engineering.

8. Conclusions and perspectives

In this review, we have described in some detail several physical and chemical properties of large organic molecules adsorbed on metal surfaces. Most of the studies on the interaction between molecular overlayers and metal substrates described in the present work were carried out by STM, which has become a unique tool to probe local phenomena on the nanometer scale. We have shown that upon landing on a surface, complex molecules often adopt conformations that are influenced by the chemical and geometric properties of the substrate of choice. The possibility of using the STM to manipulate large molecules has been extensively reviewed. In the case of Cu-TBPP, conformational changes induced by the STM tip indicated that such molecules could perform as a nanoscale switch. We showed that the adsorption of large organic molecules on metal surfaces can be associated with a local disruption of the metal substrate. The STM has been used to directly reveal such restructuring processes in many different cases, including CuPc on Ag(1 1 0) [88], C_{60} on several surfaces [19,20,44,47,109–111], and finally, HtBDC [45,46] and Lander [41,48] molecules adsorbed on Cu(1 1 0). Perhaps the most outstanding example is given by the Lander molecule, which behaves as a molecular template, reshaping portions of step edges into metallic nanostructures. The local nature of the molecule-induced surface disruption shows that such interaction can only be observed by a local probe like the STM. Finally, the growth of SAMs of several complex molecules on metal surfaces is reported [44–47,116].

As described in the section on surface diffusion, it was recently pointed out [42] that molecular diffusion properties can be effectively engineered by appropriate molecular design. The results show that the varying molecular bonding strength to the surface has consequences not only for *static* aspects of adsorption (the structure of the adsorbate monolayer and the underlying surface, which may undergo a restructuring process) but also for the dynamic behavior of the adsorbates (activation energy for diffusion and jump length). By raising the aromatic plane common to DC/HtBDC away from the surface by means of spacer groups in the case of HtBDC, this molecule has a diffusion constant which is approximately four orders of magnitude higher compared to that of its related molecule (DC) on the same surface. This observation is very important for the development of high quality organic films, since diffusivity is a key parameter for controlling film growth.

The spontaneous surface restructuring formed underneath largish molecules when adsorbed on metallic substrates is a generic way to reduce the mobility of the molecules and optimize their binding energy to the surface, even at low coverages.

In relation to restructuring processes induced by molecules possessing spacer groups (HtBDC and Lander) the driving force behind this phenomenon appears to be the strong attraction between the molecules' π-system and the surface. This attraction causes a severe distortion of the molecules' conformation, leading to an approach of the conducting backbone towards the substrate, similarly to what is observed in the conformational changes of porphyrin-based molecules on different metal surfaces. The overall strong molecule–substrate interaction, which was

somewhat weakened by the presence of spacer groups, is restored by the approach between the π-system and the surface.

A more thorough understanding of the underlying forces and mechanisms of adsorption processes holds the promise of exploiting these phenomena in a controlled manner, for example by using specially designed molecules. This may ultimately lead to new methods of nanostructuring surfaces with atomic precision, and of nanofabricating templates by using supramolecular structures. More generally, using appropriately designed molecules, the results we described point to new self-fabrication processes at the nanoscale, with potential applications ranging from integrated nanoelectronics to asymmetric catalysis.

Acknowledgements

We acknowledge financial support from the EU through the IST Project "BUN" and the TMR Network "AMMIST". We thank the Danish National Research Council for support through the Center for Atomic Scale Materials Physics (CAMP). F.R. acknowledges partial support from the EU through a Marie Curie Individual Fellowship, and from the Province of Québec through an FCAR individual grant. F.R. is grateful to R. Paynter for helpful discussions and to T.W. Johnston for a critical, in depth reading of the manuscript. Finally, we are indebted to J.V. Barth, S.W. Hla, F. Moresco, and T. Zambelli for providing their original figures, reproduced in this work.

References

[1] T. Ito, S. Okazaki, Nature 406 (2000) 1027.
[2] C. Joachim, J.K. Gimzewski, A. Aviram, Nature 408 (2000) 41.
[3] M.A. Reed, J.M. Tour, in: Computing with Molecules, Sci. Am. 6 (June) (2000).
[4] F. Moresco, G. Meyer, K.H. Rieder, H. Tang, A. Gourdon, C. Joachim, Phys. Rev. Lett. 86 (2001) 672.
[5] A. Kühnle, T.R. Linderoth, B. Hammer, F. Besenbacher, Nature 415 (2002) 891.
[6] A. D'Amico, C. Di Natale, A. Macagnano, F. Davide, A. Mantini, E. Tarizzo, R. Paolesse, T. Boschi, Biosens. Bioelectron. 13 (1998) 345.
[7] Y. Harima, T. Kodaka, H. Okazaki, Y. Kanugi, K. Yamashita, H. Ishii, K. Seki, Chem. Phys. Lett. 240 (1995) 345.
[8] T.J. Savenijc, E. Moons, G.K. Boschloo, A. Goossens, T.J. Schaafsma, Phys. Rev. B 55 (1997) 9685.
[9] M.P. O'Neill, M.P. Niemczyk, W.A. Svec, D. Gosztola, G.L. Gaines III, M.R. Wasielewski, Science 257 (1992) 63.
[10] S. Das, A.J. Pal, Phys. Stat. Sol. A 185 (2001) 383.
[11] T. Sano, H. Fujii, Y. Nishio, Y. Hamada, H. Takahashi, K. Shibata, Synth. Met. 91 (1997) 27.
[12] B. Kahr, R.W. Gurney, Chem. Rev. 101 (2001) 893.
[13] L. Schmidt-Mende, A. Fechtenkötter, K. Müllen, E. Moons, R.H. Friend, J.D. MacKenzie, Science 293 (2001) 1119.
[14] F.J. Meyer zu Heringsdorf, M.C. Reuter, R.M. Tromp, Nature 412 (2001) 517.
[15] J.V. Barth, J. Weckesser, C. Cai, P. Gunter, L. Burgi, O. Jeandupeux, K. Kern, Angew. Chem. Int. Ed. 39 (2000) 1230.

[16] A.K. Boal, F. Ilhan, J.E. DeRouchey, T. Thurn-Albrecht, T.P. Russell, V.M. Rotello, Nature 404 (2000) 746.
[17] O. Marchenko, J. Cousty, Phys. Rev. Lett. 84 (2000) 5363.
[18] M. Furukawa et al., Surf. Sci. 445 (2000) L58.
[19] J.K. Gimzewski, S. Modesti, R.R. Schlittler, Phys. Rev. Lett. 72 (1994) 1036.
[20] P.W. Murray, M.Ø. Pedersen, E. Laegsgaard, I. Stensgaard, F. Besenbacher, Phys. Rev. B 55 (1997) 9360.
[21] V.J. Langlais, R.R. Schlittler, H. Tang, A. Gourdon, C. Joachim, J.K. Gimzewski, Phys. Rev. Lett. 83 (1999) 2809.
[22] R. Rinaldi, R. Cingolani, K.M. Jones, A.A. Baski, H. Morkoc, A. Di Carlo, J. Widany, F. Della Sala, P. Lugli, Phys. Rev. B 63 (2001) 075311.
[23] H. Proehl, M. Toerker, T. Fritz, F. Sellam, K. Leo, Ch. Simpson, K. Müllen, Phys. Rev. B 63 (2001) 205409.
[24] M. Toerker, T. Fritz, H. Proehl, R. Gutierrez, F. Großmann, R. Schmidt, Phys. Rev. B 65 (2002) 245422.
[25] T.A. Jung, R.R. Schlittler, J.K. Gimzewski, H. Tang, C. Joachim, Science 271 (1996) 181.
[26] T.A. Jung, R.R. Schlittler, J.K. Gimzewski, Nature 386 (1997) 696.
[27] F. Moresco, G. Meyer, K.H. Rieder, P. Jiang, H. Tang, C. Joachim, Surf. Sci. 499 (2002) 94.
[28] T. Zambelli, H. Tang, J. Lagoute, S. Gauthier, A. Gourdon, C. Joachim, Chem. Phys. Lett. 348 (2001) 1.
[29] G. Binnig, H. Röhrer, Ch. Gerber, E. Weibel, Phys. Rev. Lett. 50 (1983) 120.
[30] H. Röhrer, Surf. Sci. 299/300 (1994) 956.
[31] F. Besenbacher, Rep. Prog. Phys. 59 (1996) 1737.
[32] F. Rosei, R. Rosei, Surf. Sci. 500 (2002) 395.
[33] B. Voigtländer, Surf. Sci. Rep. 43 (2001) 127.
[34] M. Schunack, F. Rosei, F. Besenbacher, in: A. Mendez Vilas (Ed.), Science, Technology and Education of Microscopy: An Overview, in: The Scanning Tunneling Microscope as a Unique Tool to Investigate the Interaction Between Complex Molecules and Metal Surfaces, FORMATEX Microscopy Book Series, January 2003, 43–51.
[35] S.W. Hla, L. Bartels, G. Meyer, K.H. Rieder, Phys. Rev. Lett. 85 (2000) 2777.
[36] D.M. Eigler, E.K. Schweizer, Nature 344 (1990) 524.
[37] J.A. Stroscio, D.M. Eigler, Science 254 (1991) 1319.
[38] Ph. Avouris, Acc. Chem. Res. 28 (1995) 95.
[39] J. Kliewer, R. Berndt, S. Crampin, Phys. Rev. Lett. 85 (2000) 4936.
[40] S. Zöphel, J. Repp, G. Meyer, K.H. Rieder, Chem. Phys. Lett. 310 (1999) 145.
[41] F. Rosei, M. Schunack, P. Jiang, A. Gourdon, E. Laegsgaard, I. Stensgaard, C. Joachim, F. Besenbacher, Science 296 (2002) 328.
[42] M. Schunack, T.R. Linderoth, F. Rosei, E. Laegsgaard, I. Stensgaard, F. Besenbacher, Phys. Rev. Lett. 88 (2002) 156102.
[43] T.R. Linderoth, S. Horch, E. Laegsgaard, I. Stensgaard, F. Besenbacher, Phys. Rev. Lett. 78 (1997) 4978.
[44] J. Weckesser, J.V. Barth, K. Kern, Phys. Rev. B 64 (2001) 161403.
[45] M. Schunack, L. Petersen, A. Kuehnle, E. Laegsgaard, I. Stensgaard, I. Johannsen, F. Besenbacher, Phys. Rev. Lett. 86 (2001) 456.
[46] M. Schunack, E. Laegsgaard, I. Stensgaard, I. Johannsen, F. Besenbacher, Angew. Chem. Int. Ed. 40 (2001) 2623.
[47] J. Weckesser, C. Cepek, R. Fasel, J.V. Barth, F. Baumberger, T. Greber, K. Kern, J. Chem. Phys. 115 (2001) 9001.
[48] M. Schunack, F. Rosei, Y. Naitoh, P. Jiang, A. Gourdon, E. Laegsgaard, I. Stensgaard, C. Joachim, F. Besenbacher, J. Chem. Phys. 117 (2002) 6259.
[49] M.Ø. Pedersen, P.W. Murray, E. Lægsgaard, I. Stensgaard, F. Besenbacher, Surf. Sci. 389 (1997) 300.
[50] G.P. Lopinski, D.J. Moffatt, D.D.M. Wayner, R.A. Wolkow, J. Am. Chem. Soc. 122 (2000) 3548.

[51] P. Kruse, E.R. Johnson, G.A. DiLabio, R.A. Wolkow, Nano Lett. 2 (2002) 807.
[52] G.P. Lopinski, D.D.M. Wayner, R.A. Wolkow, Nature 406 (2000) 48.
[53] P.H. Lu, J.C. Polanyi, D. Rogers, J. Chem. Phys. 111 (1999) 9905.
[54] P.H. Lu, J.C. Polanyi, D. Rogers, J. Chem. Phys. 112 (2000) 11005.
[55] P. Sautet, Chem. Rev. 97 (1997) 1097.
[56] P. Sautet, C. Joachim, Chem. Phys. Lett. 185 (1991) 23.
[57] P. Sautet, C. Joachim, Surf. Sci. 271 (1992) 387.
[58] C. Chavy, C. Joachim, A. Altibelli, Chem. Phys. Lett. 214 (1993) 569.
[59] C. Goletti, A. Sgarlata, N. Motta, P. Chiaradia, R. Paolesse, A. Angelaccio, M. Drago, C. Di Natale, A. D'Amico, M. Cocco, V.I. Troitsky, Appl. Phys. Lett. 75 (1999) 1237.
[60] A. Sgarlata, A. Angelaccio, N. Motta, R. Paolesse, C. Di Natale, A. D'Amico, Surf. Sci. 466 (2000) 167.
[61] M. Magoga, C. Joachim, Phys. Rev. B 57 (1998) 1820.
[62] J.M. Tour, Chem. Rev. 96 (1996) 537.
[63] A. Gourdon, Eur. J. Org. Chem. 2797–2801 (1998).
[64] C. Viala, A. Secchi, A. Gourdon, Eur. J. Org. Chem. (2002) 4185.
[65] J. Kuntze, R. Berndt, P. Jiang, H. Tang, A. Gourdon, C. Joachim, Phys. Rev. B 65 (2002) 233405.
[66] T. Zambelli, P. Jiang, J. Lagoute, S.E. Grillo, S. Gauthier, A. Gourdon, C. Joachim, Phys. Rev. B 66 (2002) 075410.
[67] A.J. Heinrich, C.P. Lutz, J.A. Gupta, D.M. Eigler, Science 298 (2002) 1381.
[68] T.W. Fishlock, A. Oral, R.G. Egdell, J.B. Pethica, Nature 404 (2000) 743.
[69] L. Bartels, G. Meyer, K.H. Rieder, Phys. Rev. Lett. 79 (1997) 697.
[70] A. Kühnle, G. Meyer, S.W. Hla, K.H. Rieder, Surf. Sci. 499 (2002) 15.
[71] F. Moresco, G. Meyer, K.H. Rieder, H. Tang, A. Gourdon, C. Joachim, Appl. Phys. Lett. 78 (2001) 306.
[72] W. Ho, Acc. Chem. Res. 31 (1998) 567.
[73] L.J. Lauhon, W. Ho, Phys. Rev. Lett. 84 (2000) 1527.
[74] H.J. Lee, W. Ho, Science 286 (1999) 1719.
[75] K.D. Dobbs, D.J. Doren, J. Chem. Phys. 97 (1992) 3722.
[76] T. Yokoyama, S. Yokoyama, T. Kamikado, Y. Okuno, Nature 413 (2001) 619.
[77] G.L. Kellogg, Surf. Sci. Rep. 21 (1994) 1.
[78] B.S. Swartzentruber, Phys. Rev. Lett. 76 (1996) 459.
[79] J. Weckesser, J.V. Barth, K. Kern, J. Chem. Phys. 110 (1999) 5351.
[80] J.V. Barth, Surf. Sci. Rep. 40 (2000) 75.
[81] J.L. Brand, M.V. Arena, A.A. Deckert, S.M. George, J. Chem. Phys. 92 (1990) 5136.
[82] D.C. Senft, G. Ehrlich, Phys. Rev. Lett. 74 (1995) 294.
[83] J. Yoshinobu, H. Tanaka, T. Kawai, M. Kawai, Phys. Rev. B 53 (1996) 7492.
[84] M. Doering, H.P. Rust, B.G. Briner, A.M. Bradshaw, Surf. Sci. 410 (1998) L736.
[85] W. Fan, X.G. Gong, W.M. Lau, Phys. Rev. B 60 (1999) 10727.
[86] B.C. Stipe, M.A. Rezaei, W. Ho, Science 279 (1998) 1907.
[87] J.K. Gimzewski, C. Joachim, R.R. Schlittler, V. Langlais, H. Tang, I. Johannsen, Science 281 (1998) 531.
[88] M. Bohringer, R. Berndt, W. Schneider, Phys. Rev. B 55 (1997) 1384.
[89] M. Giesen-Seibert, R. Jentjens, M. Poensgen, H. Ibach, Phys. Rev. Lett. 71 (1993) 3521.
[90] G.M. Whitesides, B. Grybowski, Science 295 (2002) 2418.
[91] F. Schreiber, Prog. Surf. Sci. 65 (2000) 151.
[92] A.N. Shipway, E. Katz, I. Willner, Chem. Phys. Chem. 1 (2000) 18.
[93] M.O. Lorenzo, C.J. Baddeley, C. Muryn, R. Raval, Nature 404 (2000) 376.
[94] B. Kasemo, J. Gold, Adv. Dent. Res. 13 (1999) 8.
[95] C.A. Mitchell, L. Yu, M.D. Ward, J. Am. Chem. Soc. 123 (2001) 10830.
[96] A.A. Dhirani, R.W. Zehner, R.P. Hsung, P.G. Sionnest, L.R. Sita, J. Am. Chem. Soc. 118 (1996) 3319.
[97] R. Staub, M. Toerker, T. Fritz, T. Schmitz-Hübsch, F. Sellam, K. Leo, Langmuir 14 (1998) 6693.

[98] A. Kühnle, S. Vollmer, T.R. Linderoth, G. Witte, C. Wöll, F. Besenbacher, Langmuir 18 (2002) 5558.
[99] S. Prato, L. Floreano, D. Cvetko, V. De Renzi, A. Morgante, S. Modesti, F. Biscarini, R. Zanoni, C. Taliani, J. Phys. Chem. B 103 (1999) 7788.
[100] F. Biscarini, R. Zamboni, P. Samorì, P. Ostoja, C. Taliani, Phys. Rev. B 52 (1995) 14868.
[101] V.M. Kenkre, F. Biscarini, C. Bustamante, Phys. Rev. B 51 (1995) 11074.
[102] M. Furukawa, H. Tanaka, K. Sugiura, Y. Sakata, T. Kawai, Surf. Sci. 445 (2000) L58.
[103] M. Böhringer, K. Morgenstern, W.-D. Schneider, M. Wühn, Ch. Wöll, R. Berndt, Surf. Sci. 444 (2000) 199.
[104] M.A. Reed, C. Zhou, C.J. Muller, T.P. Burgin, J.M. Tour, Science 278 (1997) 252.
[105] H. Park, J. Park, A.K.L. Lim, E.H. Anderson, A.P. Alivisatos, P.L. McEuen, Nature 407 (2000) 57.
[106] G. Gensterblum, K. Hevesi, B.Y. Han, L.M. Yu, J.J. Pireaux, P.A. Thiry, R. Caudano, A.A. Lucas, D. Bernaerts, S. Amelinckx, G. Van Tendeloo, G. Bendele, T. Buslaps, R.L. Johnson, M. Foss, R. Feidenhans, G. Le Lay, Phys. Rev. B 50 (1994) 11981.
[107] P.A. Bruhwiler, A.J. Maxwell, P. Baltzer, S. Andersson, D. Arvanitis, L. Karlsson, N. Mårtensson, Chem. Phys. Lett. 279 (1997) 85.
[108] A.J. Maxwell, P.A. Brühwiler, S. Andersson, N. Mårtensson, P. Rudolf, Chem. Phys. Lett. 247 (1995) 257.
[109] R. Fasel, P. Aebi, R.G. Agostino, D. Naumovic, J. Osterwalder, A. Santaniello, L. Schlapbach, Phys. Rev. Lett. 76 (1996) 4733.
[110] C. Cepek, A. Goldoni, S. Modesti, Phys. Rev. B 53 (1996) 7466.
[111] M. Pedio, R. Felici, X. Torrelles, P. Rudolf, M. Capozi, J. Rius, S. Ferrer, Phys. Rev. Lett. 85 (2000) 1040.
[112] A.V. Hamza, in: K.M. Kadish, R.S. Ruoff (Eds.), Fullerenes: Chemistry, Physics and Technology, Wiley, New York, 2000, p. 531.
[113] E. Giudice, E. Magnano, S. Rusponi, C. Boragno, U. Valbusa, Surf. Sci. 405 (1998) L561.
[114] C. Cepek, R. Fasel, M. Sancrotti, T. Greber, J. Osterwalder, Phys. Rev. B 63 (2001) 125406.
[115] J.A. Appelbaum, D.R. Hamann, Solid State Commun. 27 (1978) 881.
[116] M. Schunack, E. Laegsgaard, I. Stensgaard, F. Besenbacher, J. Chem. Phys. 117 (2002) 8493.
[117] G.A. Jeffrey, An Introduction to Hydrogen Bonding, Oxford University Press, New York, 1997.
[118] J.L. Atwood, J.E.D. Davies, D.D. MacNicol, F. Vögtle, J.-M. Lehn (Eds.), Comprehensive Supramolecular Chemistry, Pergamon, New York, 1996.
[119] C. Cai, M. Bösch, B. Müller, Y. Tao, A. Kündig, C. Bosshard, Z. Gan, I. Biaggio, I. Liakatas, M. Jäger, H. Schwer, P. Günter, Adv. Mater. 11 (1999) 745.
[120] C. Cai, B. Müller, J. Weckesser, J.V. Barth, Y. Tao, M.M. Bösch, A. Kündig, C. Bosshard, I. Biaggio, P. Günter, Adv. Mater. 11 (1999) 750.
[121] J.V. Barth, H. Brune, R.J. Behm, G. Ertl, Phys. Rev. B 42 (1990) 9307.
[122] K. Kern, H. Niehus, A. Schatz, P. Zeppenfeld, J. George, G. Comsa, Phys. Rev. Lett. 67 (1991) 855.
[123] D. Vanderbilt, Surf. Sci. 268 (1992) L300.